The Cassegrain ADC for Keck 1

Detailed Design Report
Revision 5
June 8, 2004

Table of Contents

1 Summary

Lick Observatory is prepared to immediately start the Fabrication and Assembly stage of this project following the Detailed Design Review and resolution of any issues that need to be closed following that review. The Work Plan and detailed drawings and schematics presented at Detailed Design are expected to form the basis of the contract from CARA for this portion of the work. This information along with the project background is available on the web at http://adc.ucolick.org//. The current schedule would have the ADC being installed on the Keck 1 telescope in mid-2005.

The Phase A Study for this project was started in October of 2001. The Preliminary design was started in March 2003 following the Phase A Reviews, and the Detailed Design Study was started in December 2003 following the PDR.

The optical glass has been ordered from Corning and delivered to Zygo, who have a contract directly from CARA to start fabrication. Zygo is expected to complete their contract in October, 2004, and the prisms will be delivered to Lick Observatory for coating. Lick plans to apply the MgF to the prisms and then to have LLNL apply a Sol-Gel coating. If required a hydrophobic coating will be applied by Lick over the Sol-Gel.

The base plan is to have LLNL coat the prisms with Sol-Gel at their facilities, as they have coated optics for several other projects for us. It is possible that they will not agree to coat these prisms, and the back-up plan is to coat them at Lick Observatory in facilities that are currently being developed. The hydrophobic coating would need to be done at Lick in any case.

We plan to purchase a majority of the bought parts soon after CARA issues a contract for the next phase. The parts are listed in the bill of materials in the mechanical and electronics sections. CARA will directly buy the instrument control computer. This project does not include an electronics box, as the plan is to mount the ADC electronics in the HIRES electronics enclosure on the right Nasymth platform of the Keck 1 telescope. There is presently room in that enclosure for these electronics, and it is planned that some of the existing electronics will be removed from that locker once the HIRES CCD is upgraded to a mosaic. The current plan is to install the mosaic this summer.

The exact hand paddle configuration and local control are not fully resolved at this point, and the design shown for this portion may change in detail. We plan to resolve this issue very soon after the Detailed Design Review, before parts are bought. The documentation will be updated to whatever is agreed upon.

2 Introduction

This report was assembled from materials resulting from the Detailed Design by the Technical Facilities Group of Lick Observatory and from materials supplied directly by CARA. The report represents the results of the Detailed Design Study. Detailed Mechanical and Electronics drawing and descriptions can be found on the ADC web site (http://adc.ucolick.org//) along with the Phase A and Preliminary Design reports and reviews.

The PDR report made a number of comments and recommendations regarding the Cassegrain ADC. Several of these are found in the body of the report. In addition a list of points to be addressed was included in the conclusions section of the PDR report.

Mechanical Design

Gravity acting on the prism cells as the telescope elevation changes will cause the prism cells to place a moment on the lead screw via the nut. The deflection produced is minimal as the lead screws are 25 mm in diameter. Cyclic loading due to the deflection is well below the endurance limit and the estimated life of the nut and bearing is not impacted. The end of each lead screw is turned down to a shaft, which passes through two bearings, so eccentric motion of the shaft end is not expected, but this will be reviewed in the detail design phase.

Vern's answer:

The design of the translation system has the ball slides supporting the moment and the ball screw providing the translation force. Most of the FEA analysis has been done with that assumption, i.e. the ball nut is constrained to the screw only in translation, not rotation. The calculations for the life of the ball slides were also done with this assumption. If you assume that the ball screw is perfectly rigid in moment and constrains the connection to the ball screw in theta x and theta y, it shares the moment load with the ball slides. An FEA analysis was run with this assumption, and found the moment load in the ball screw to be 395 in lb. This introduces a stress of 6000 psi in the ball screw, far below the endurance limit of the steel screw.

Stress Induced Birefringence

Stress induced birefringence may have an impact on precision polarimetry, Jacques Beckers recommends that the ADC design team contact Keller at the National Solar Observatory for comments on this issue. Christoph Keller is evaluating these effects for the LADC design for the LBT. In lieu of other information the best recommendation is that the ADC not be used when precision polarimetric observations are done with LRIS.

Drew's answer: *The workaround is to not use the ADC for these observations. More information may be available at the review.*

Maintainability and Reliability

The PDR charter asked a number of specific questions about the Cassegrain ADC. Question 6 was as follows:

6. Does the proposed design present any features that raise concern for maintainability and reliability?

The committee answered with the following concerns:

Answer: Yes, in two areas. First, the design should address the possibility of dust ingress to the second prism upper surface when the telescope is at zenith with the ADC installed. An effort should be made to minimize the paths for dust to reach that second prism surface. Second, the durability and aging characteristics of the Sol-gel coating should be investigated and discussed with the observatory along with cleaning procedures and requirements.

The ADC has prism cells have an Ultra-pol non-contacting seal between them and the stationary structure to keep most of the dust from the inside surfaces.

The durability and aging of the coatings are discussed in Section 4.1.2, Coatings.

Conclusions Section – Points to be addressed in Detailed Design

The following specific points were given with the recommendation that each should be addressed in the Detailed Design phase activities (the numbering matches that given on pages 9 and 10 of the PDR report):

2. A detailed assembly and alignment procedure for the ADC should be developed during the Detailed Design phase.

This is presented as Section 4.2.3, Assembly and Alignment Procedure.

4. Additional attention should be given to characterizing the coatings and confirming the transmission that will be achieved. In particular test coatings should be done to confirm the transmission and to evaluate compatibility with various cleaning procedures.

This is presented in section 4.1.2, Coatings.

5. The field flattener from the original HIRES dewar should be removed after the upgrade is complete and sent to Livermore for measurement of transmission. The original and new transmission curves can then be compared to look for aging effects. Other groups should also be contacted for information about coating durability and aging effects.

This could not be done as HIRES is still using this dewar for science. Jim Stilburn of the DAO has been contacted and is assisting us in evaluating the durability of coating. This will be covered in the future in Section 4.1.2, Coatings.

6. The effect of the ADC should be evaluated in terms of the acceptable tolerances for pointing and focusing accuracy.

This is presented as Section 4.1.3, Effect of the ADC on Pointing and Focusing.

7. Any software GUI designs required by the ADC should be defined in the detail design phase.

This is presented in Section 4.4.3, GUI designs.

3 Specifications and Requirements

3.1 Final Instrument Specifications

Please refer to
http://adc.ucolick.org/prelim_design/workplan/Cassegrain_ADC_Requirements_1.3.2.pdf

3.2 Compliance Matrix for Requirements

Please refer to
http://adc.ucolick.org/detailed_design/Report/ADC_compliance_matrix_DDR.pdf

4 Detailed Design

4.1 Optical Design

4.1.1 Design Summary

We have further developed the Linear ADC design from the time the Preliminary Design Review (PDR). Only minor changes have been made to the optical design, and so the PDR report adequately describes the modeled optical performance. In response to the PDR committee, as well as to address some missing information, several detailed areas have been investigated:

1. Anti-reflection (AR) coating design, including fabrication of some trial coatings;
2. Pointing and focus correction models; and
3. Optimum prism separation with elevation.

In addition, we attach the “figure of merit” report requested by the SSC to estimate gains to be realized with the ADC. Please see Appendix 1 for the report.

The summary of the current design and tolerances is given below:

Prism opening angle	2.5°
Prism central thickness	45 mm
Prism clear aperture	1019.2 mm (min.) + 10 mm for safety
First prism offset	-22.1 mm (below center)
Minimum prism edge thickness	22 mm
First prism angle at outer surface	1.67°
First prism angle at inner surface	-0.83°
Minimum prism separation	20 mm
Maximum prism separation	1700 mm
Location in front of telescope focal surface	1575 mm – center of ADC 680 mm – min. distance (wrt 2nd prism)
Zenith distance for full correction	0 -- 60°
Prism Material	Fused Silica (Grade D purchased)
Coatings	MgF_2 + Sol-Gel
Expected Transmission	> 92%; ≥ 94% average

Tolerances:

Tolerance in prism position, axial	10 mm
Tolerance in prism position, radial	<5mm (set by safety margin above)
Tolerance in prism angle	0.2°
Tolerance in index inhomogeneity	3×10^{-5} ($\leq 4.2\times10^{-6}$ realized)

The nominal plate scale at the Keck focus is 1.379″/mm.

4.1.2 Coatings and Expected Transmission

A two-layer coating consisting of MgF_2 plus silica Sol-Gel was selected at the PDR, and we have investigated coating design, durability and achieved performance. In practice, something very close to $\lambda/4$ of silica Sol-Gel ($n\approx1.23$) on top of $\lambda/4$ of MgF_2 ($n\approx1.38$) gives good results over a broad pass-band; the location of the pass-band is set by the choice of λ. However, we were advised by Jim Stilburn (DAO/HIA) that

1. Sol-Gel adheres poorly to MgF_2; and
2. Sol-Gel coatings tend to absorb moisture, lowering their performance over time.

Fortunately, Stilburn has identified hydrophobic agents that work well and are applied in sufficiently thin layers that they have only small effects on the optical performance.

In order to address the adhesion problem, we decided to try placing a thin (~5 nm) layer of silica between the MgF_2 and the Sol-Gel. Again, the layer is so thin that it has little effect on the optical properties of the coating. Using the new 48-in coating chamber at UCO/Lick, we deposited ~85 nm of MgF_2 and (optionally) ~4 nm of SiO_x, SiO_2 or Al_2O_3 on one side of quartz witness samples. Jim Stilburn kindly spin-coated these samples with silica Sol-Gel, and then tested the adhesion. He found that the bare MgF_2 provided poor adhesion, no matter if it had been deposited by e-gun or resistance boat. The samples with

bond layers all had good adhesion. (Stilburn's adhesion tests are to rub the coatings several times with a dry, folded Kim-wipe, applying considerable finger pressure, and then to examine the coating under magnification; this is repeated as needed until damage becomes apparent. He describes adhesion with the silicon oxides "nearly as good as for bare glass", and with the sapphire "tough as nails".) However, SiO_x was later found to absorb too strongly in the UV for our use. In addition, one of the three SiO_2-bond layer samples failed in adhesion (most likely due to an error in the evaporative coating process), so some further investigation is needed. Sapphire may be the bond layer of choice, although its higher index of refraction makes it less desirable than silica from an optical standpoint. While the final choice of bond layer has not been made, we consider the adhesion problem solved.

Following the adhesion tests, we coated two 3-mm thick quartz witness samples with ~78 nm of MgF_2 and ~4 nm of SiO_2 on each side, and asked Jim Stilburn to deposit a quarter-wave of Sol-Gel tuned to 440 nm on top of this. This tuning wavelength is slightly shorter than optimal, but we wished to demonstrate that the optical properties of these coatings in the UV are adequate. One sample ("B") had a layer of hydrophobic agent applied to both sides as well. This agent had a somewhat larger effect than expected, as the transmission measured by Stilburn before the agent was applied showed sample B to be slightly better than A, whereas measurements afterwards showed B to be significantly poorer than A. Stilburn reports that the layer of hydrophobic agent was probably too thick.

Using the transmission of these two samples, as measured at UCO/Lick with a Cary 5000 spectrophotometer, and Corning's transmission curve for the fused silica, we have estimated the total ADC transmission assuming 4 surfaces with AR coating and 90 mm of quartz. The results are shown in Figure 1. We see that the transmission is ≥92.5% everywhere except for a small dip (in the glass) near 944 nm, and even here it is ≥91.5%. We consider these to be conservative expectations of the eventual transmission, as the final coating should be tuned to slightly better performance and the final hydrophobic layer will be thinner.

At this point, the plan is for UCO/Lick to apply all layers except the Sol-Gel, which will be dip-coated at LLNL. UCO/Lick is developing a Sol-Gel coating facility at this time, but it is unlikely to be fully operational on the timescale required by the ADC.

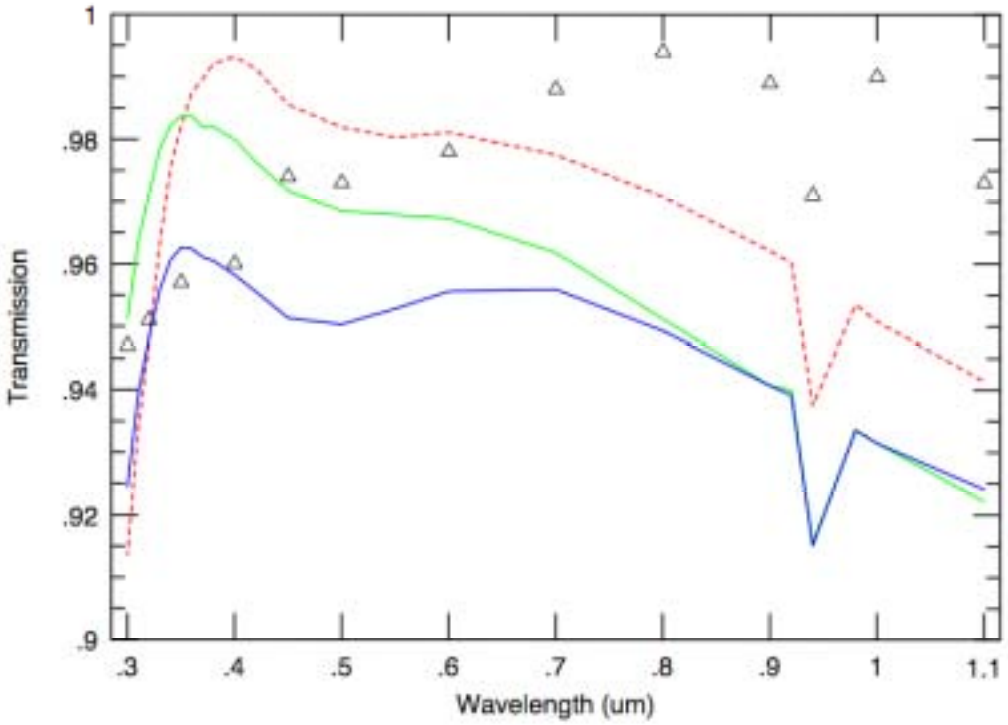

Figure 4.1-1: Expected throughput of the total ADC, based on 90-mm of quartz and 4 surfaces as measured from demonstration samples A (green) and B (blue). Also shown is the theoretical curve assuming the ideal Sol-gel thickness (red). The triangles are the transmission values estimated at the time of the PDR.

4.1.3 Pointing and Focus Adjustments

Pointing:
As the prisms separate, the image at the telescope focal surface is displaced and the telescope must be re-pointed in order to place the image at the same location. During observations, this displacement will automatically be corrected by the guider. However, the pointing adjustment will be needed during field acquisition.

ZEMAX was used with an on-axis image to estimate the pointing adjustment, which is purely a function of prism separation:
$\Delta\theta = 2.807 \times 10^{-2} \cdot \Delta d + 1.15$
where $\Delta\theta$ is the pointing adjustment in arcseconds towards lower elevation, and Δd is the prism separation in mm. (Note: there is a significant chance that the sense of this adjustment is incorrectly stated!)

Focus adjustment:
Since the focal surface is curved, as the prisms separate and the focal surface is displaced an effective tilt in the focal surface is introduced. The best focus has been estimated using ZEMAX at Fields 1, 3 and 5 (i.e., angles 0, 90 and 180 degrees; see PDR report) with several prism separations, and using the slitmask as the focal surface. The results are slightly more complicated than expected, probably due to the effects of image aberrations introduced by the ADC. However, the focus adjustment is dominated by prism separation (Δd) and instrument angle ($\Delta\phi$), as expected. The following formula for the adjustment to secondary piston is good to ±3-μm over the range of parameters explored:

$$\Delta z = (a \cdot \cos\phi + b) \cdot \Delta d + c$$

$$a = -2.6726 \times 10^{-5}; b = 7.353 \times 10^{-6}; c = -1.3492$$

where Δz is in microns (negative means away from the primary), and Δd is in mm.

4.1.4 Prism Separation with Elevation

The dispersion correction made by varying the prism separation as a function of elevation only. Using ZEMAX and a set of wavelengths spanning the working range, we have derived the following numbers from which an interpolation formula of look-up table may be derived:

Z (deg)	Half Separation (mm)		**Z (deg)**	Half Separation (mm)
3	12.58		**50**	580.43
4	21.32		**52.5**	635.81
8	56.56		**54**	672.13
12	92.50		**55**	697.82
16	129.54		**56**	724.80
20	168.07		**57**	753.20
24	206.61		**58**	783.16
28	251.75		**59**	814.81
32	298.20		**60**	848.34
36	348.88		**61**	883.93
40	404.97			
42.5	443.43			
45	485.08			
47.5	530.50			

4.1.5 Update on Index of Refraction Inhomogeneities

Corning has cast and sawed the blank that will be used for the ADC prisms. They measured inhomogeneities in the refractive index across a 23-in beam through the pre-sawn blank, and reported peak-to-peak inhomogeneities of 4.2×10^{-6} (maximum) and $\sim2\times10^{-6}$ (typical). These are well within our tolerance, producing ray deflections ≤0.7-μm at the telescope focal plane in the worst case.

4.2 Mechanical Design

4.2.1 Design Summary

This report presents the detail design of the Cassegrain ADC for Keck I.

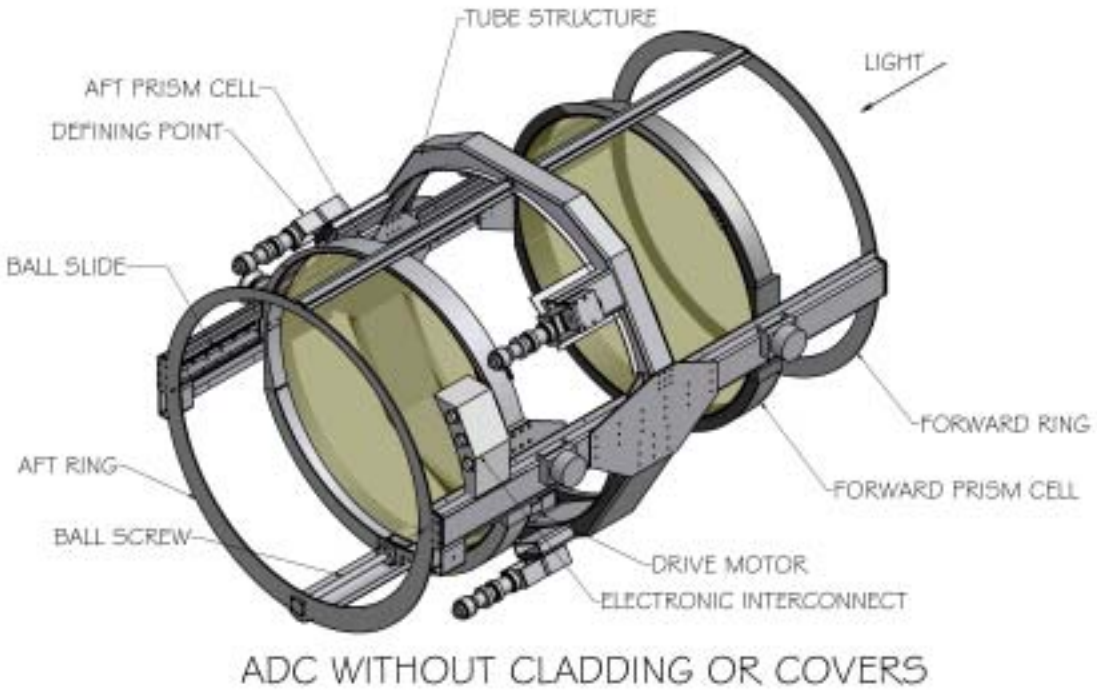

Figure 4.2-1: Cassegrain ADC without cladding or covers.

As in the preliminary design the prisms move toward and away from the center of the instrument, maintaining a constant center of gravity. This design incorporates a single ball screw to control prism separation, with two ball slides maintaining perpendicularity and lateral placement of the prisms to the optical axis. The structural components are rectangular tube to support the moment loads generated by the ball screw located near the edge of the optics. The structure and cell materials are steel to meet the thermal and stiffness requirements of the design.

The ball screws are left hand thread on the aft prism and right hand on the forward prism. These are driven from the center by a Galil motor, gearbox and toothed belt. Since, at any time one prism is being lifted while the other is being lowered, the net torque to move the prisms is only the torque required to overcome friction. The ball screw drive has been moved from the top of the instrument (pointed at the horizon) to the bottom to gain

clearance on the chain drive used to install forward Cassegrain instruments. The prism separation range is from 20 to 1700 mm.

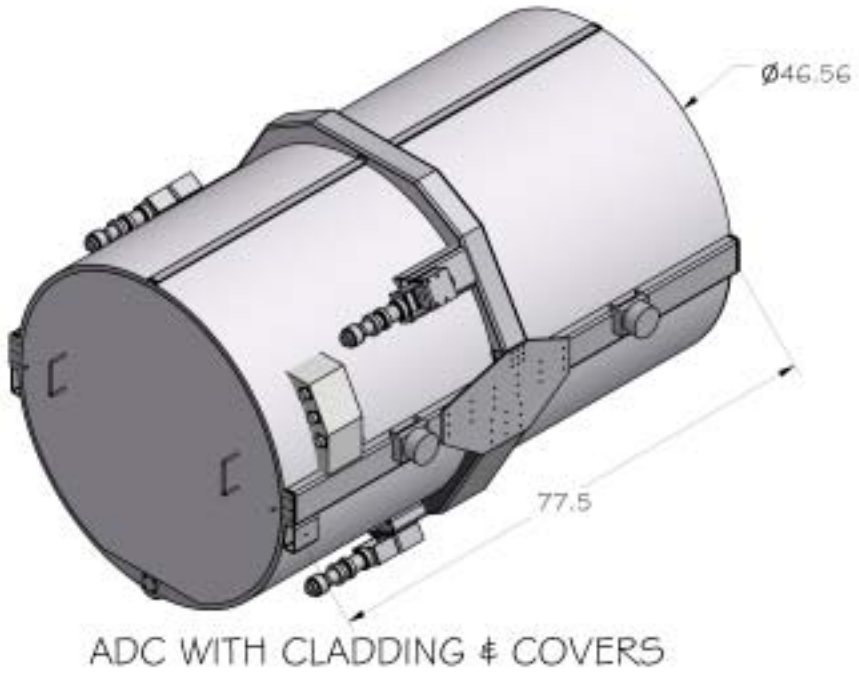

Figure 4.2-2: ADC with cladding and covers.

The cladding and covers are aluminum. The inside is flocked with Ultra-Pol, a black adhesive backed polishing fabric.

4.2.1.1 Location, Weight and Mounting

The total instrument weight is 1250 lbs. The electronics will be mounted in the Hires electronics vault.

The instrument will mount into the tertiary tower on defining points to be installed be Keck. The locations of these points have been agreed to between Keck and Lick and are specified in the ICD. The Z position of the instrument is in front of LRIS and must clear the front hatch of LRIS. Keck is going to revise this hatch from a door to a sliding hatch.

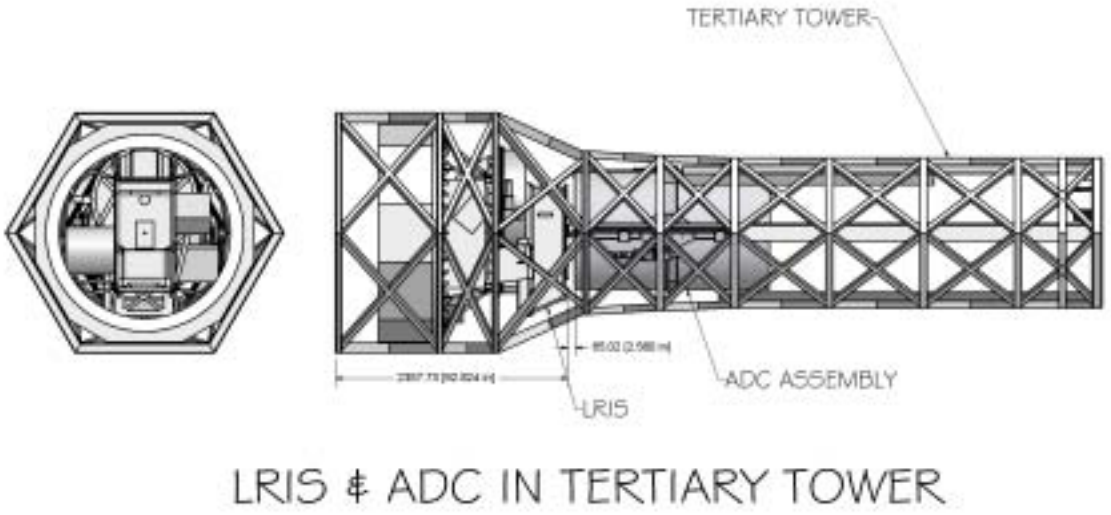

Figure 4.2-3: LRIS & ADC in tertiary tower

The instrument will be stored in and installed through the Cassegrain Transfer Module. The locations of the defining points have been chosen so that they do not interfere with the transfer module. The defining points are back (+Z) of the center of gravity of the instrument to clear the baffle deployment assemblies in the tertiary tower. When the transfer module is in use for other instruments the ADC will be stored on a Jack Stand permanently mounted on the nasmyth deck.

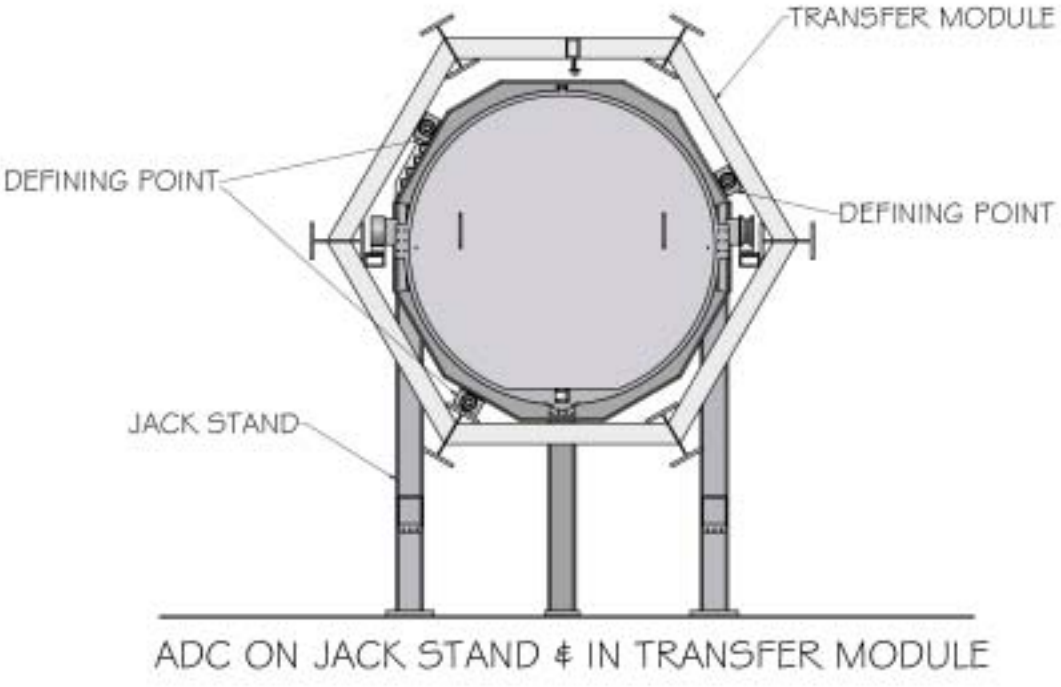

Figure 4.2-4: ADC on jack stand in transfer module

4.2.1.2 Jack Stand Design

The jack stand mounts permanently on the nasmyth deck behind the module handler for the transfer module. It has 2 long forks that extend under the ball slide support tubes for the aft optic and have dowels that key into the support tubes. These lift the ADC free of the rails in the transfer module by pivoting upward. The pivot is actuated manually with an acme screw. An FEA analysis of the stand has been done and the lowest natural frequency is 10.1 hz.

Seismic restraint is achieved by capturing the fork with a tube, and by a dowel pin in each fork that key into the instrument.

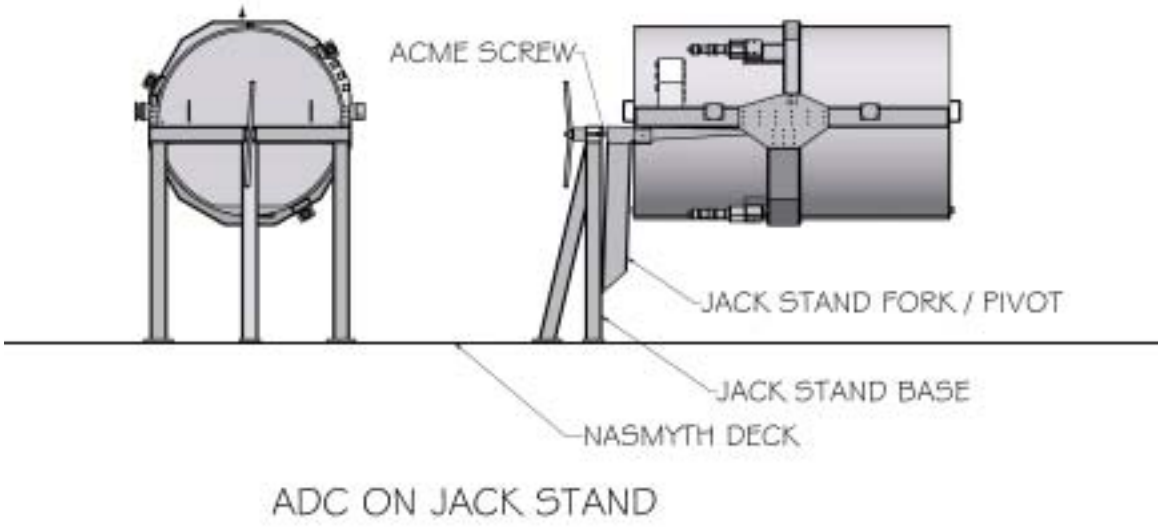

Figure 4.2-5: ADC On Jack Stand

4.2.1.3 Cell Design

The prisms are mounted in steel cells with three radial and three axial constraints at 120 degrees. These constraints have adequate clearance to accommodate the temperature variation specified in the ICD.

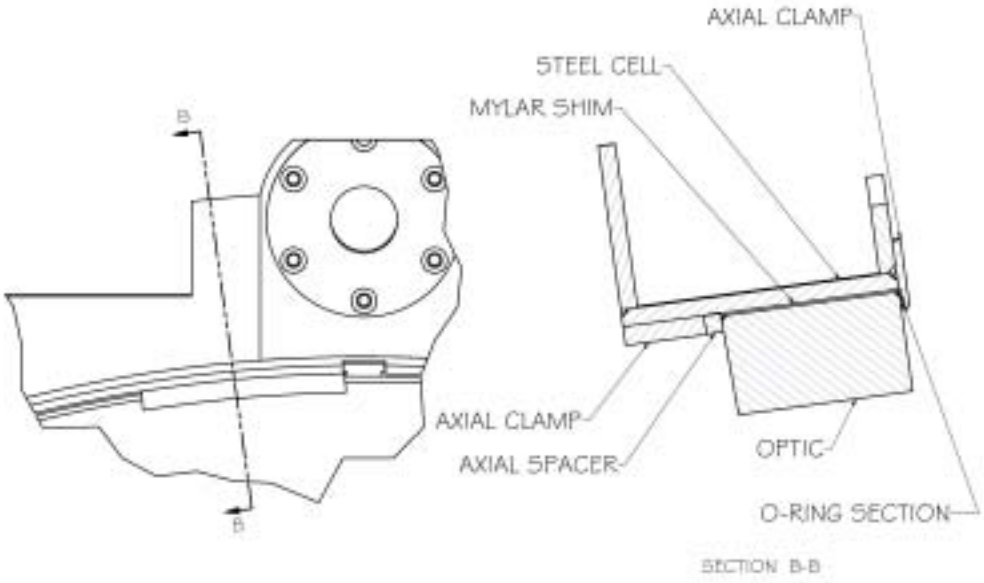

Figure 4.2-6: Cutaway View of Optic Mount

The section of o-ring just provides some spring loading to hold the optic against the axial clamp. It is on the upper surface of each optic when pointed at the zenith.

The inner surfaces of the prisms are parallel to each other and tilted 0.83 degrees to the optical axis. The tilt is accomplished by mounting the ball slides at a 0.83-degree angle from axis of the cell. The ball slide mount pads are bolted onto the cell and also hold the index tab for the fiducal/limit sensors.

4.2.1.4 Structure

The stiffness requirements for the structure are met by constructing the base structure from rectangular tube. A finite element analysis of the final structure has been preformed. The stresses are all within allowable levels for the materials used. The deflections of the prisms from desired locations have been predicted. The results of this analysis are reported in the Structural Analysis Section (4.2.2).

4.2.1.5 Mechanisms

The moment load resulting from a single ball screw placed at the edge of the prism cell is taken by the ball slides. As a result each cell has have slide / rail assemblies with 2 slides on each one. The slides are separated by 7" centers to accept the moment. We have identified and obtained quotes on slides from 2 manufacturers that meet the requirements.

The ball screw diameter is constrained partly by the manufacturers ability to manufacture one of adequate length. The ball screw diameter is 25 mm diameter screw. There are separate screws at each end of the instrument. These are coupled at the center and constrained axially and radially by bearings near the coupling. The outer ends are constrained radially by bearings. The center coupling is also the timing belt pulley.

The design of the translation system has the ball slides supporting the moment and the ball screw providing the translation force. Most of the FEA analysis has been done with that assumption, i.e. the ball nut is constrained to the screw only in translation, not rotation. The calculations for the life of the ball slides were also done with this assumption. If you assume that the ball screw is perfectly rigid in moment and constrain the connection to the ball screw in theta x and theta y, it shares the moment load with the ball slides. An FEA analysis was run, with this assumption, and found the moment load in the ball screw to be 395 in lb. This introduces a stress of 6000 psi in the ball screw, well below the endurance limit of the steel screw.

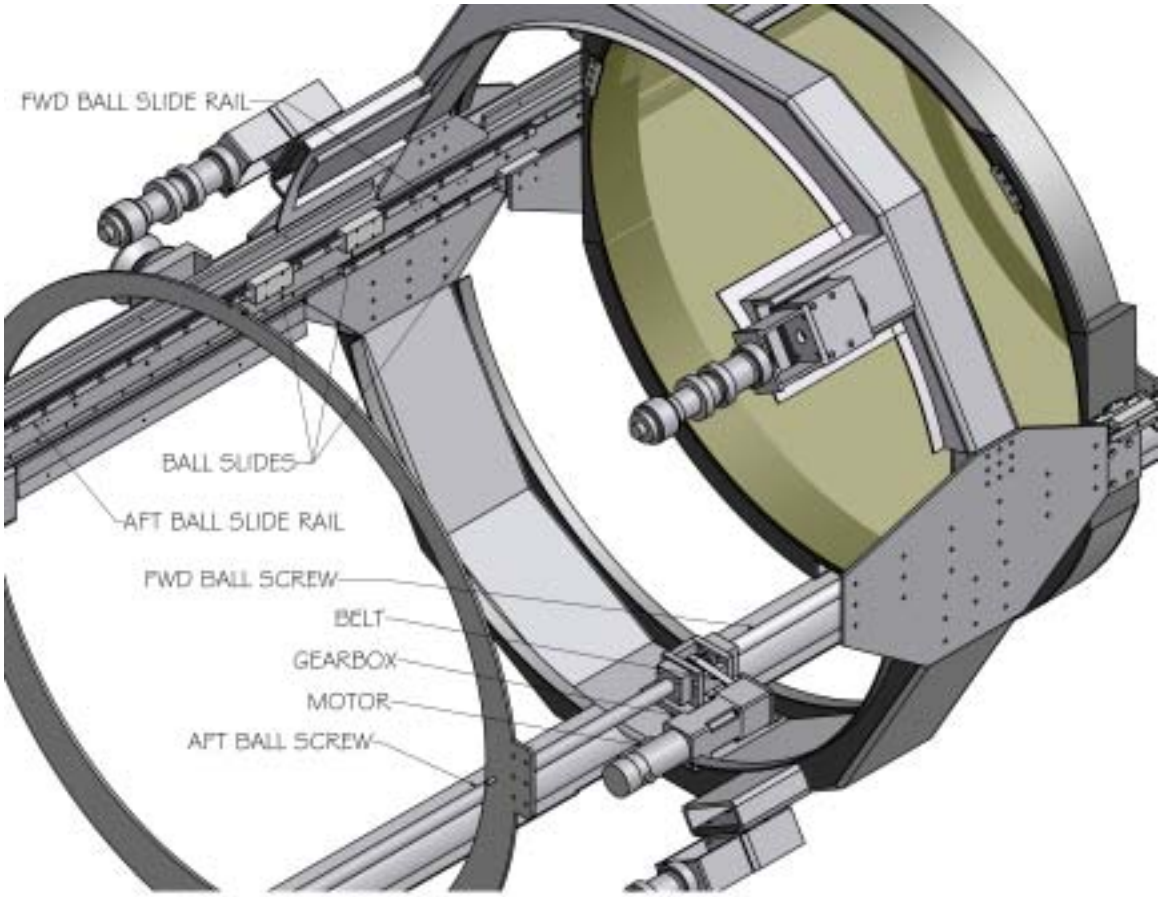

Figure 4.2-7: Shown without aft cell assembly

The motor is a Pitman servomotor controlled by a Galil controller. A Bayside 10:1 gearbox provides speed reduction and a timing belt connects to the ball screw.

4.2.1.6 Mechanical Performance

The maximum travel rate for an individual prism is 20 mm/sec. This allows the correction adjustment of the ADC to keep up with the telescope slew rate at 60 degrees zenith distance. The maximum separation of the inner surfaces of the prisms is 1700 mm and the minimum separation is 20 mm.

The positional accuracy is limited by flexure of the instrument. The positional deflections due to gravity are less than 2 mm. The optical tolerance on separation distance is 20 mm. The positional deflections due to gravity are presented in the structural analysis.

Maximum power to the motor is expected to be 10 W. This will be dissipated by the motor and the mechanical components of the instrument. We do not expect this to be significant. This is less than the 50 W maximum specified in the requirements document.

4.2.1.7 Encoder, fiducal, and limit locations, mounting and logic

A rotary encoder is installed on the front of the instrument, attached to the forward ball screw. This is used by software to determine that the drive system is functioning properly. The fiducals and limits are Hall effect sensors that are mounted along the ball slide support tube between the ball slides on one side of the instrument.

The fiducal will be closer to the end of travel, in the maximum correction direction, than the length of the index tab. When the instrument powers up, if the fiducal is blocked by the tab the cell will move toward the center of the instrument, otherwise it will move outward. A complete description of the logic and wiring is provided in drawing EL-3610.

4.2.1.8 Testing at Santa Cruz

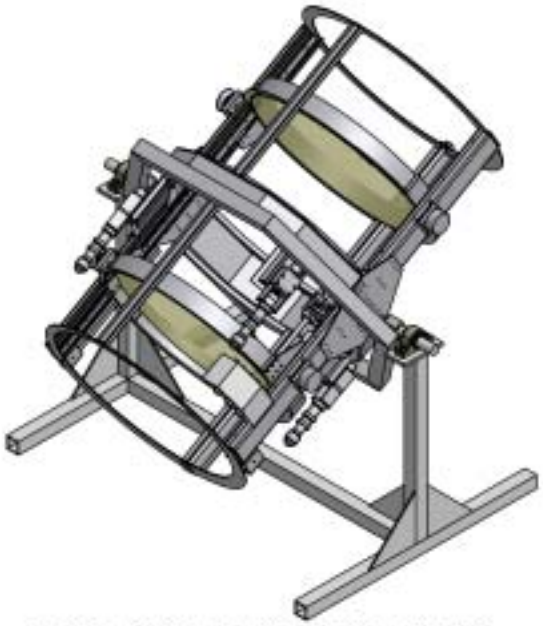

Figure 4.2-8: ADC on test stand, shown without cladding

We plan to construct a stand for the assembly, alignment and test of the ADC. We expect to use the actual defining points for this work. See Alignment and Test Plan.

4.2.2 Structural Analysis

A finite element analysis of the entire structure has been run. This models the structural tubes as plate shell elements, parts of the prism cells as solids, and uses some beam elements to tie things together. The optics were modeled as solids with a single element through the thickness. They are held in the cells by x,y,z constraints at one point at each mounting pad. Since the pads are actually 3" long, this over-predicts the stresses; however, constraining at additional points introduces moments that are not representative of the actual mounting scheme. The cladding was included in the analysis.

The coordinate axis for this analysis, with the instrument at the horizon is: z along the optical axis (+ in direction of light travel), y vertical (+ down), x horizontal (+ left when looking at back of instrument).

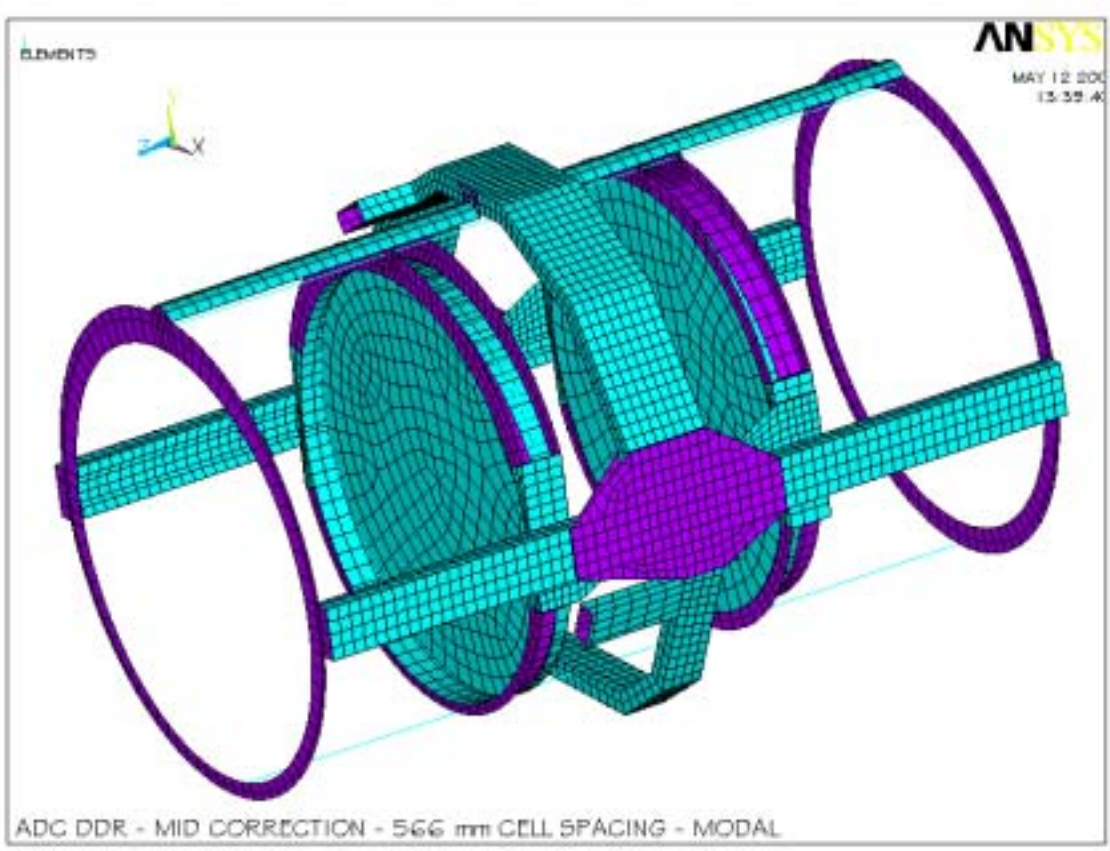

Figure 4.2-9: ADC without cladding.

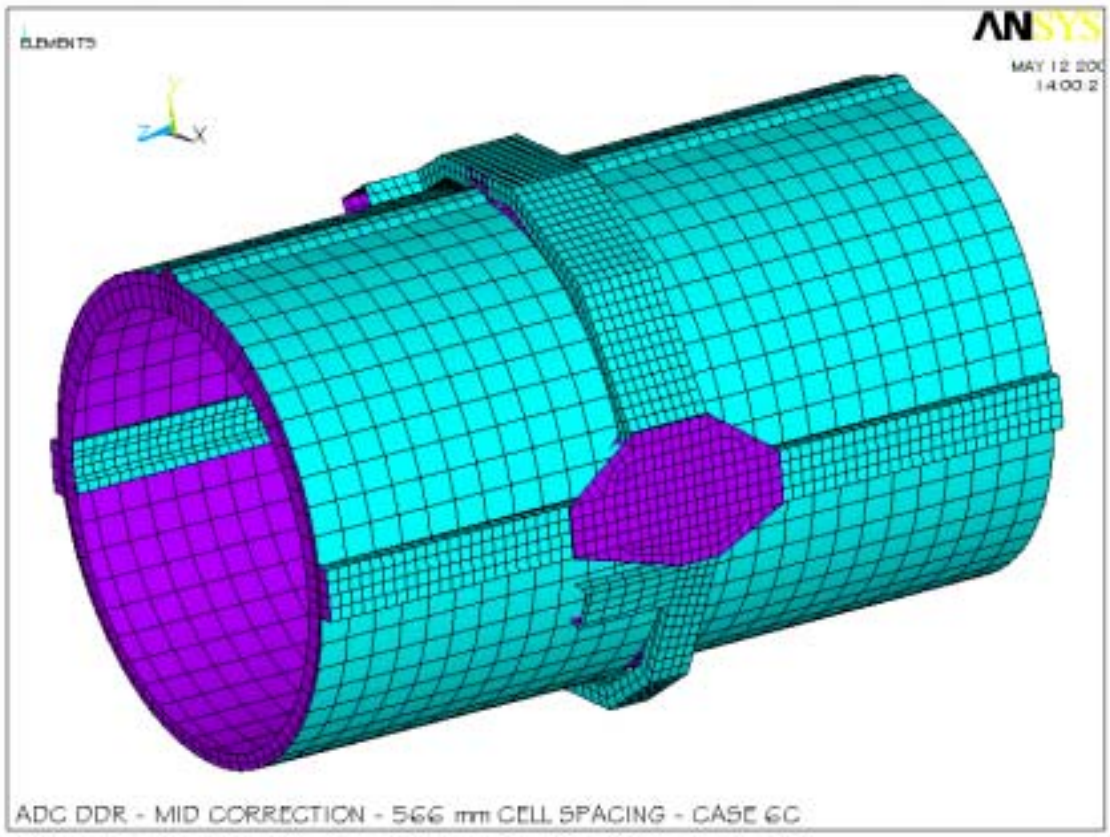

Figure 4.2-10: ADC with Cladding

A modal analysis and various gravity loads were run. The gravity loadings were:

1) Instrument at zenith with full dispersion correction. This is a worst case, not an operating mode.
2) Instrument at zenith with null correction
3) Instrument at 30 degrees from zenith at the 30-degree correction, 566 mm prism separation.
4) Instrument at 60 degrees from zenith at full correction, 1700 mm prism separation.
5) Instrument at horizon at full correction. Full correction will be the normal observing mode from 60 degrees zenith distance to the limits of telescope travel.
6) An analysis was run with an arbitrary 10-pound load applied axially on the ball slides of one side of the optic only. This was to simulate friction on one set of slides. The loads and stresses were well within tolerances.

The first 25 modal frequencies are:

Table 4.2-1

MODE	FREQ	
1	13.925	FWD Cell theta y
2	14.686	FWD Cell theta x
3	15.296	AFT Cell theta y
4	16.056	AFT Cell theta x
5	44.327	
6	48.841	
7	59.389	
8	63.811	
9	64.159	
10	66.744	
11	69.137	
12	72.632	
13	72.744	
14	74.053	
15	74.257	
16	76.530	
17	78.881	
18	79.275	
19	80.058	
20	81.825	
21	82.702	
22	82.969	
23	83.553	
24	84.617	
25	84.895	

The four lowest modes are rotations of the optic cells. At 13.9 hz minimum, the assembly is adequately stiff.

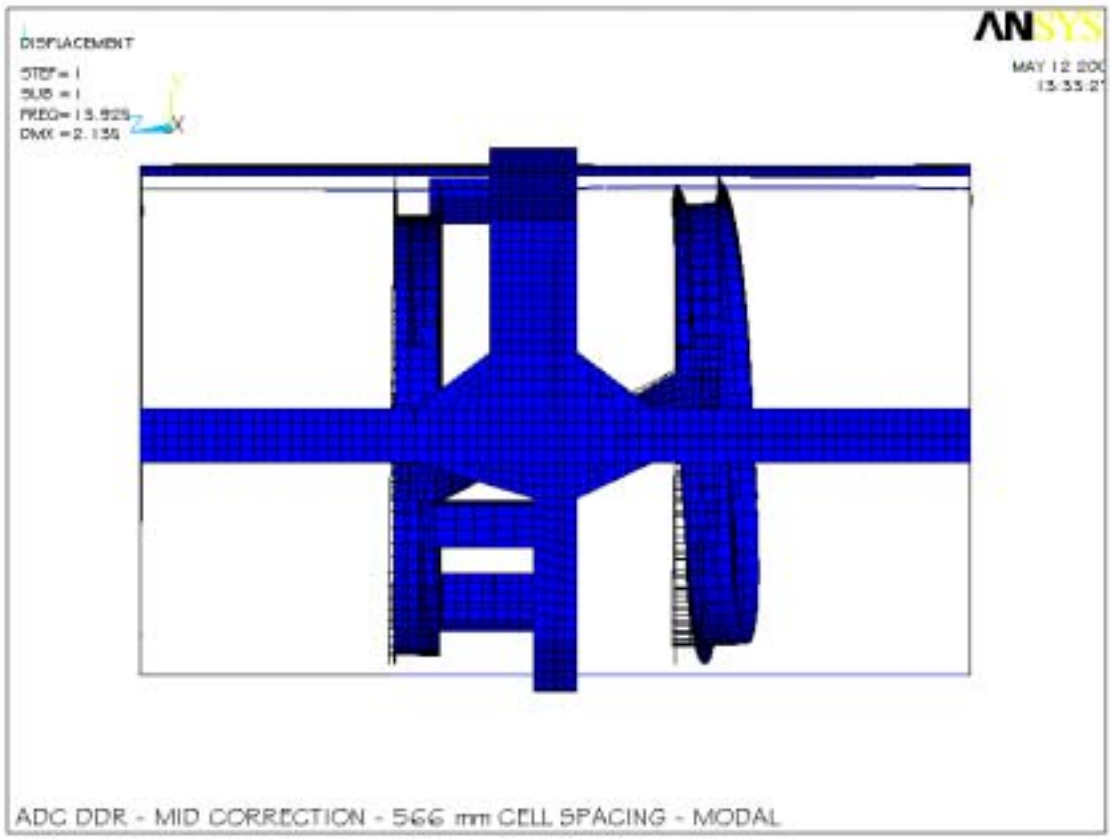

Figure 4.2-11: Mode #1, side view, 13.9 hertz, theta y rotation of forward cell.

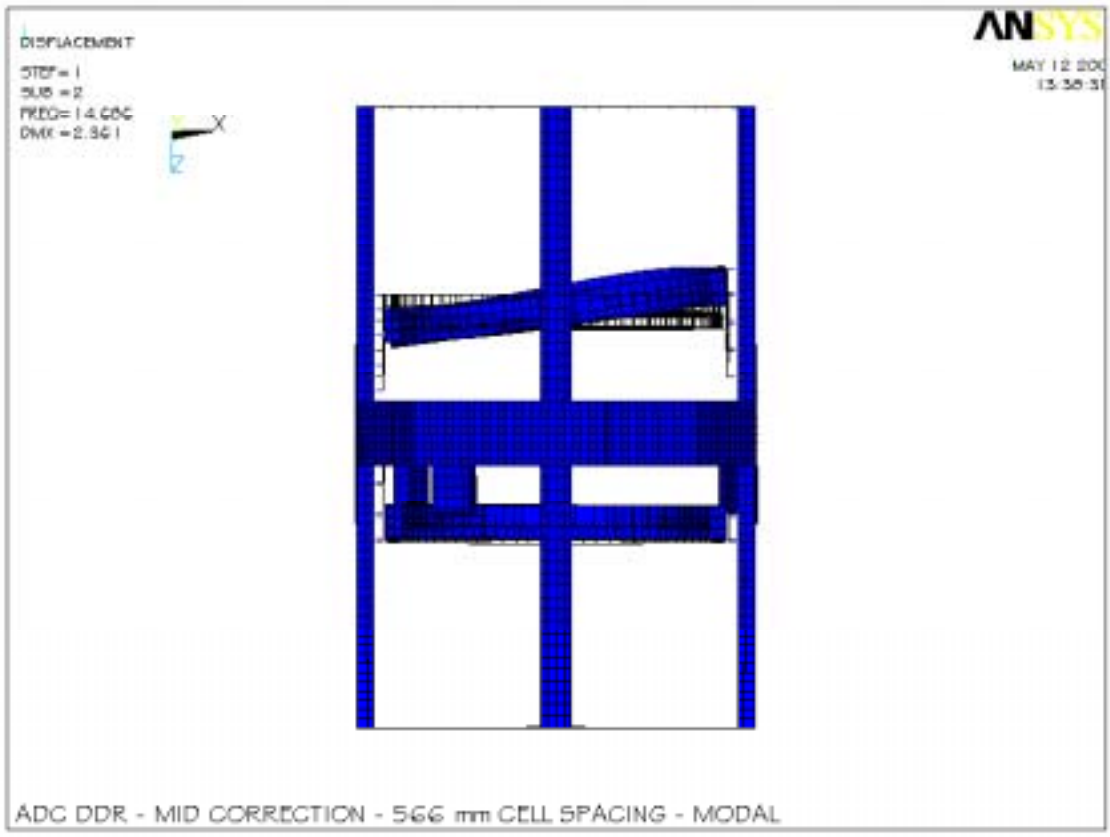

Figure 4.2-12: Mode #1, top view, 13.9 hertz, theta y rotation of forward cell.

The zenith gravity load with null correction gives the worse case deflection of the prisms. The largest deflection is a tilt of 1.6 mm across the diameter. This is a theta x rotation. These are both in the same direction; therefore the inner surfaces of the prisms stay nearly parallel. Their relative tilt is .3 mm across the diameter, (0.02 degrees). The most stringent optical constraint is the relative tilt between the inner surfaces of the two optics. This shows up as ROTX and ROTY in the data presented. The optical tolerance is 0.2 degrees.

The deflections of the optics in several modes are provided below. They are all within the optical requirements.

The deflections of the center of the prisms at zenith and full correction are:

Table 4.2-2

FULL CORRECTION (1700 MM) AT ZENITH						
OPTIC CENTER	UX (mm)	UY (mm)	UZ (mm)	ROTX (deg)	ROTY (deg)	ROTZ (deg)
AFT OPTIC	-0.02	-0.04	1.07	-0.076	0.007	-0.005
FWD OPTIC	0.02	0.02	1.05	-0.076	0.005	-0.004
Difference	-0.04	-0.02	0.02	0.00	0.002	-0.001

The deflections during operation at zenith are:

Table 4.2-3

20 MM CORRECTION AT ZENITH						
OPTIC CENTER	UX (mm)	UY (mm)	UZ (mm)	ROTX (deg)	ROTY (deg)	ROTZ (deg)
AFT OPTIC	-0.02	-0.03	0.97	-0.068	0.010	-0.001
FWD OPTIC	0.02	0.01	1.14	-0.085	0.010	0.001
Difference	-0.04	-0.04	-0.17	0.017	0.000	-0.002

The deflections during operation at 30 degrees zenith angle are:

Table 4.2-4

566 MM CORRECTION AT 30 DEGREE ZENITH ANGLE						
OPTIC CENTER	UX (mm)	UY (mm)	UZ (mm)	ROTX (deg)	ROTY (deg)	ROTZ (deg)
AFT OPTIC	-0.02	-0.01	0.87	-0.063	0.008	-0.001
FWD OPTIC	0.01	0.03	0.97	-0.073	0.007	0.000
Difference	-0.03	-0.04	-0.1	0.010	0.001	-0.001

The deflections during operation at 60 degrees zenith angle are:

Table 4.2-5

FULL CORRECTION (1700 MM) AT 60 DEGREE ZENITH ANGLE						
OPTIC CENTER	UX (mm)	UY (mm)	UZ (mm)	ROTX (deg)	ROTY (deg)	ROTZ (deg)

AFT OPTIC	-0.02	0.04	0.57	-0.042	0.003	-0.001
FWD OPTIC	0.01	0.08	0.48	-0.033	0.002	0.000
Difference	-0.02	-0.04	0.09	-0.009	0.001	-0.001

The deflections of the optics at the horizon and full correction are:

Table 4.2-6

FULL CORRECTION (1700 MM) AT HORIZON						
OPTIC CENTER	UX (mm)	UY (mm)	UZ (mm)	ROTX (deg)	ROTY (deg)	ROTZ (deg)
AFT OPTIC	-0.01	0.07	0.04	-0.004	-0.001	-0.000
FWD OPTIC	0.00	0.08	-0.05	0.006	-0.001	0.000
Difference	-0.01	-0.01	--0.09	-0.010	0.000	0.000

A finite element model of the optic constrained at 3 points similar to the current mounting scheme was run to predict stresses and deflections in the glass. Since these constraints are at points instead of spread out over the three-inch mounting pad, this is a conservative approach.

The stresses in the aft optic at the zenith are:

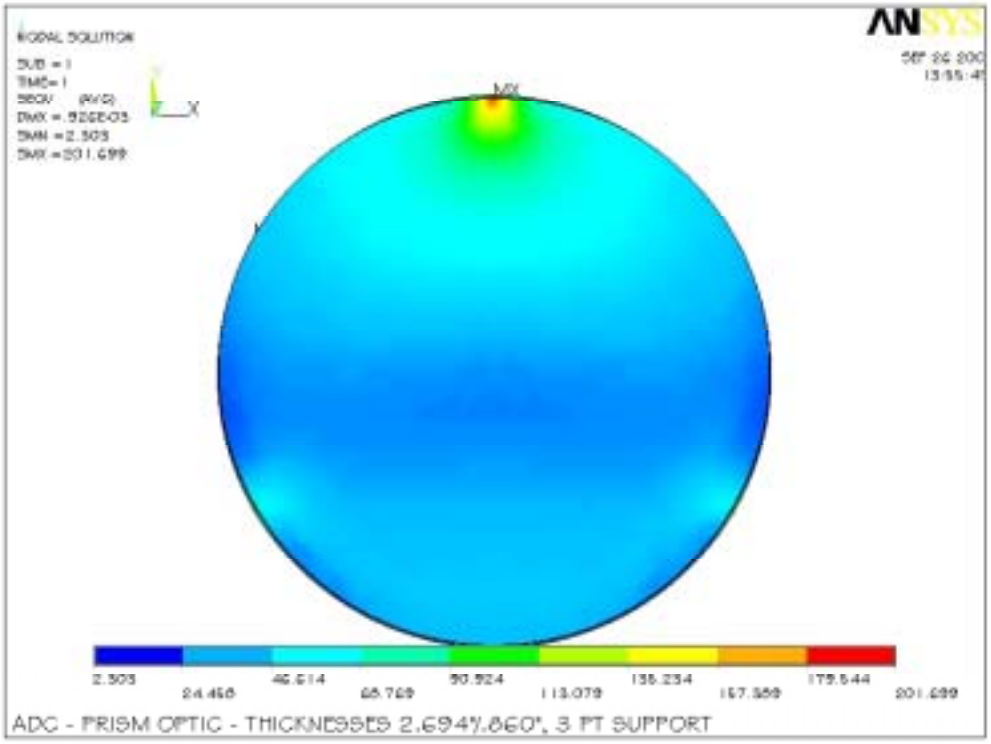

Figure 4.2-13

The stresses in the forward optic at the zenith are:

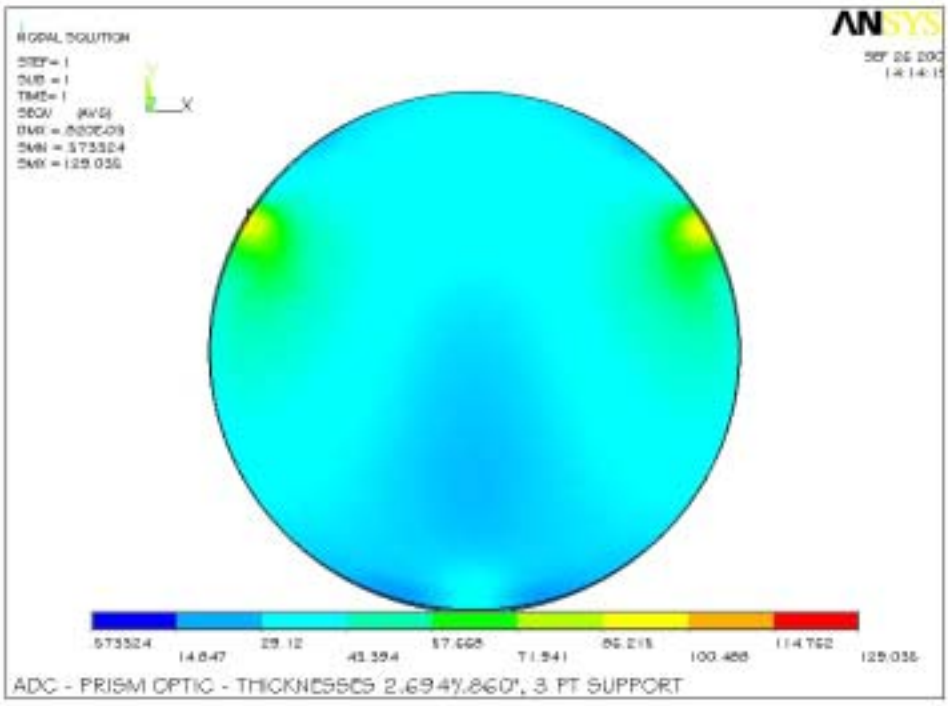

Figure 4.2-14

Deflection of the aft optic due to gravity, looking at zenith:

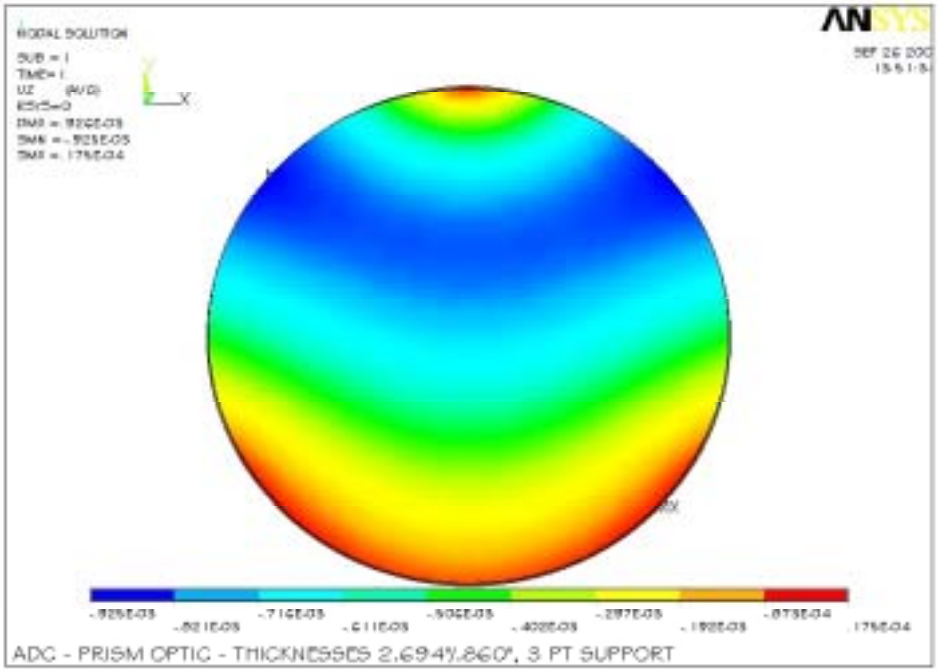

Figure 4.2-15

Deflection of the forward optic due to gravity, looking at zenith:

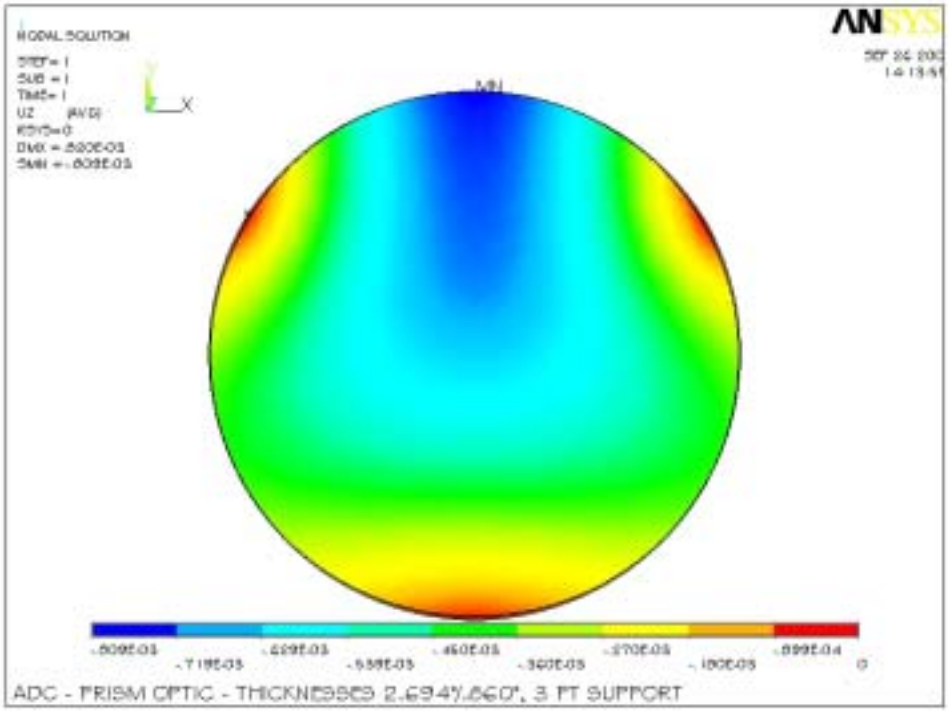

Figure 4.2-16

Stresses in steel looking at zenith angle of 30 degrees and 566 mm correction are:

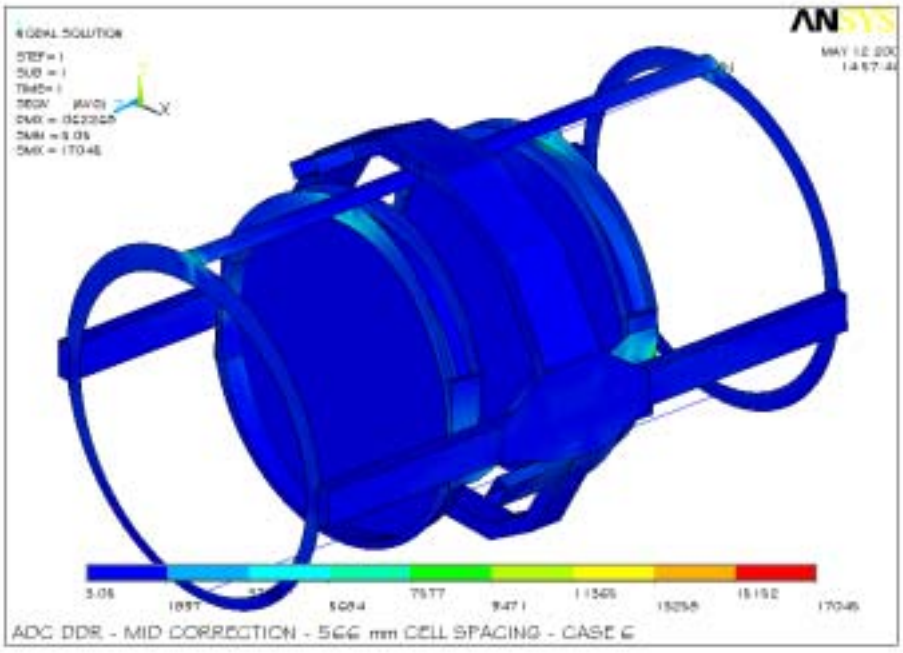

Figure 4.2-17

The highest stresses are in the plates that the ball slides mount on and are an artifact of the modeling of the ball slides. The highest actual stresses are below 7,000 psi. These are well below the yield stress of mild steel, 36,000 psi.

4.2.3 Assembly and Alignment

4.2.3.1 Assembly and Internal Alignment Procedure

The ADC structure will be built and assembled by the Lick Shops. This will include installation and alignment of the prism cells and the mechanisms. The mechanisms will be tested, including initial tuning of the controller.

We plan to make dummy optics from aluminum plate. These will weigh as much as the final optics and install into the cells in the same manner. The aft optic will have a hole in the center and a hole near the edge with provisions for a cross hair reticle. The forward optic will have the same holes offset 22.1 mm to account for the prism offset. These will be machined accurately enough to act as alignment tools. We also plan to build an assembly / test stand (A8001) and a prism assembly fixture (A8060).

After the ADC is assembled and installed on the test fixture, the dummy optics will be installed using the same procedure that will be used for the real prisms. A detailed procedure has been written for this. The servo will be tuned and the final alignment checks will be performed. These will consist of installing a crosshair at each end of the instrument on permanently installed pins and using an alignment scope to determine that the center and axis of travel of each prism is in the correct position relative to the center of the instrument. The reticles near the edge of the prisms will be used to confirm that the relative rotation of the prisms is within tolerance and that they stay within tolerance during translation from null to full correction. Life tests and vibration tests also be done at this time. An engineer from Keck will perform vibration tests.

The dummy optics will be removed and the optics will be installed after the mechanical testing is complete. We expect to ship the instrument to Keck with the optics installed.

4.2.3.2 Alignment to the Telescope

Since the optics of the ADC do not have any power, their alignments to the telescope in translation are constrained only by mechanical and vignetting considerations. The rotation tolerance for the forward prism about the optical axis is +-0.75 degree. The rotation tolerances about the other two axis are 0.2 degree. The translation constraint along the optical axis of the telescope of +-6 mm prevents mechanical interference with LRIS and has no effect on vignetting. The translation tolerance perpendicular to the optical axis is set at 5 mm in any direction by the clear aperture of the optics.

The alignment theory will be to align the ADC with an axis in the telescope defined by the center of rotation of LRIS and the center of the secondary mirror. This prevents vignetting

of the LRIS field of view and provides a line to set the rotation of the ADC to that is well within the 0.2 degree optical tolerance.

We plan to build a fixture that will mount kinematically in front of LRIS and hold a cross hair that is adjustable. This fixture must be thin enough to mount between LRIS and ADC. We also plan to provide pins to mount crosshairs on both ends of ADC to establish the center axis of the instrument and a provision to place a level to establish rotation about the optical axis.

These will be used to align ADC with the following procedure:

1) Mount the crosshair fixture and define LRIS in the tertiary tower with a person in the tower. That person aligns the cross hair to the center of LRIS rotation, using a marking pin to establish the center of LRIS rotation.
2) Remove LRIS and the cross hair fixture.
3) Install ADC, with cross hairs on both ends and install the cross hair fixture.
4) Set up an alignment scope on the deck and use the three cross hairs and the spot at the center of the secondary to align the ADC in x and y translation and theta x and theta y rotation.
5) Use a tape measure to establish z translation (along the optical axis). This can
6) Use a level to establish theta z rotation (around the optical axis). A precision level will read to 0.024 degree.

Both the establishment of the telescope axis and the alignment of the ADC to that axis should be doable to 1 mm for a total alignment accuracy of approximately 1.5 mm. This is well within the 5 mm tolerance.

4.3 Electrical Design

4.3.1 Design Summary

The ADC electronics consist of a 19” rack mounted control box and the prism stage mounted equipment. At the prism stage the following components move and monitor the stage position:

- DC Servomotor with encoder
- Load encoder
- Limit and *HOME* Hall-effect switches

As shown on the block diagram, schematic EL-3601, sheet 1, the control electronics consist of:

- Interconnect panel
- Network hub
- AC power controller
- Galil DMC-2210 servomotor controller
- Galil AMP-19520 servo amplifier

- Galil IOM-1964 64-channel I/O module
- 24V Power supply
- Lick interlock box

Starting at the left side of the diagram, the interconnect panel will actually consist of the three front panels on the electronics box. The first panel, the output panel, holds the connectors for connecting to the ADC stage. The second panel holds the connectors for the observatory E-Stop signal, the emergency null paddle, and the local/remote paddle and is part of the interlock box. The last panel, the input panel, holds the various communications connectors and the AC power input connector.

Communications:
The only connection required to talk to the ADC electronics is the network cable connected the control computer. This connection is made on the input panel via a ruggedized RJ45 connector. This connector is similar to a standard bayonet style MS connector but it also allows for use of a standard RJ45 connector if needed. The serial connectors on the input panel are there for troubleshooting problems. They include serial connections directly to the Galil controller and to the Pulizzi power controller. The two network jacks are wired to the network hub contained if the electronics box and provide a convenient outlet for a laptop computer.

AC Power:
The input AC power is connected to the electronics box via a front panel mounted RFI input module. This module is wired to the Pulizzi power controller and the network hub. The network hub is wired directly to the AC input. This ensures that the hub will power up whenever power is applied to the box and that communications with the Pulizzi are possible at all times.

The Pulizzi power controller is used to give software control of power cycling of the Galil controller, the 24 volt power supply, and the interlock system. The Pulizzi also allow power up and power down sequencing via the setting of variable if desired.

Instrument control:
The ADC control system is built around the Galil DMC-2210 servomotor controller. The controller generates the drive signal and monitors the status of the instrument. The status consists of primary and secondary limits, stage *HOME* signal, interconnection of cable signals, and various monitor inputs such as ambient temperature and 24V power level. The motor signal is sent to the servo amplifier that amplifies the power to the motor. The gain of the amplifier is jumper selected for 1.0 Amp/volt. This drive signal is then wired to the ADC stage motor shown via the interlock system. If no lock out conditions exist, the motor power continues on to the stage on the right hand side of the sheet. The amplifier module also contains interconnect screw terminals for the various limits switches and encoder inputs.

64-Channel I/O module:
The extended I/O module connects to the Galil controller and accept the input signals from the extra limit switches, cable connected signals, and emergency stop signals. The only output used at this time is a pulse that is sent to a timer circuit that will indicate a network or hardware error on an LED on the interlock front panel. If the circuit is not continuously pulsed, the LED will be lite indicating that the controller is not generating the pulse.

Interlock box:
The interlock system performs the following functions:

- Disconnects power to the motor if a secondary limit is tripped
- Manages the Local/Remote function
- Allows for the use of the emergency null paddle
- Sends status information back to the controller

Most importantly, the interlock system controls the power flowing to the stage motor. If an error conditions occurs, the interlock system will open the appropriate relay disconnecting motor power. If a secondary limit is the cause of the error, the interlock system will allow a movement (retract) toward the null position by plugging in the emergency null paddle. The Local/Remote function allows a technician to control the ADC motion either from a hand paddle of from the front panel of the electronics box. When selected for remote operation a set of two pushbuttons are available to manually move the stage. The controller is sent a signal that the paddle/front panel is in use and will not attempt to move the stage. Note that the local movement mode removes the restrictions of the software and primary limits. The secondary limits are the only functioning limits in this mode.

The status sent back to the controller includes the position of the local/remote switch, the secondary limits, the emergency and E-Stop inputs, and the connection of the emergency null paddle.

ADC Stage:
The ADC stage consists of two co-operating prism cells. Each cell runs in opposite directions as the stage is commanded to move. The null position is the position where the prisms are closest to each other. The stage limits, as defined by the Galil controller, are mounted to the forward prism cell. These are the primary limits, the *HOME* signal and the secondary limits. A subset set of limits is also mounted to the aft prism cell but these are only used to provide position information/conformation. That is, the aft cell *HOME* signal should also be active when the forward cell *HOME* signal is active. The same applies to the aft cell secondary limits. The aft cell does not have primary limits because a motor stage can only have one set of primary limits.

A second, or load, encoder is mounted to the end of the ball screw that drives the two cells. This is a lower resolution encoder that is used to verify motion at the ball screw when the motor is commanded to move.

4.3.2 Interconnect List

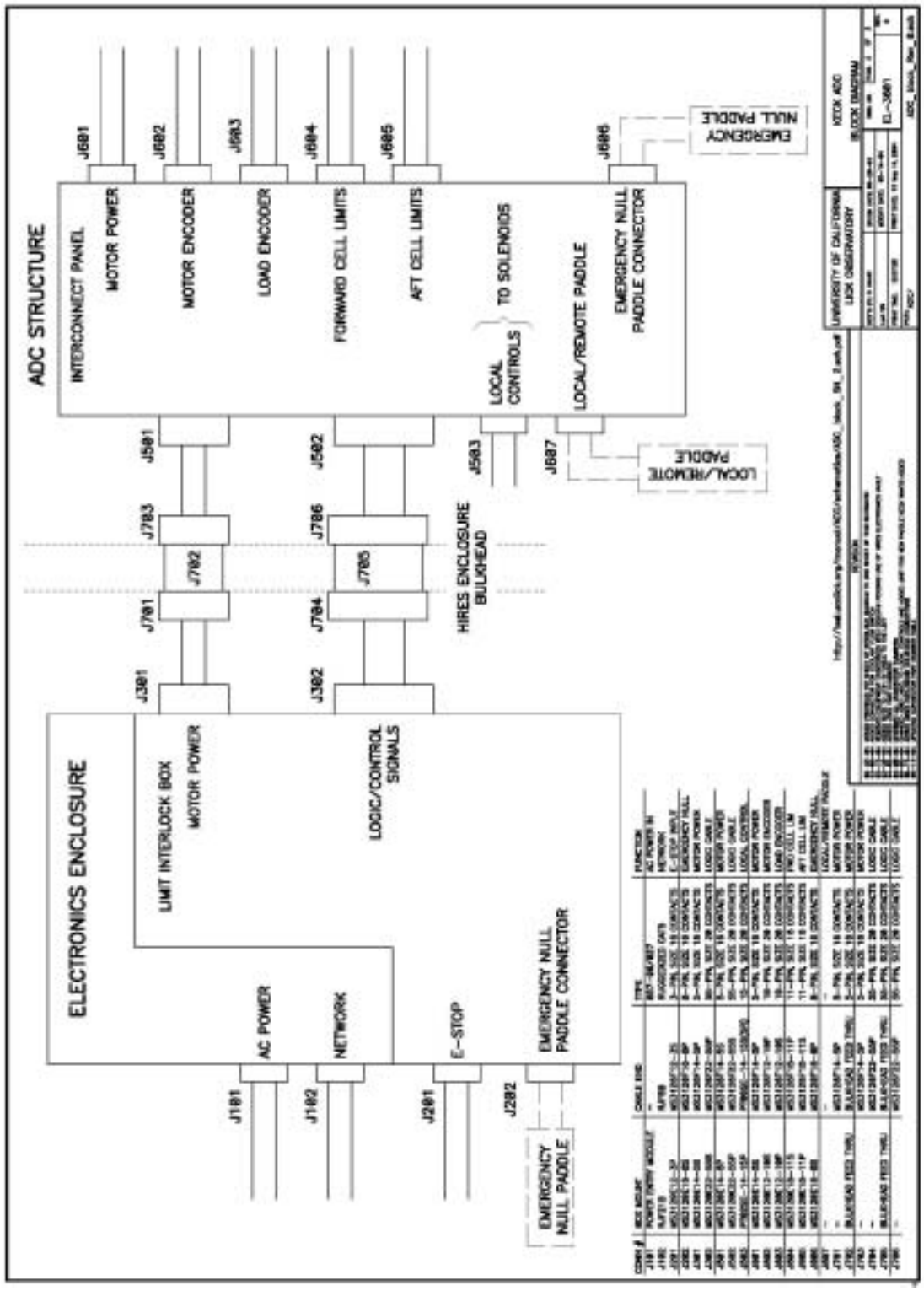

4.4 Software

4.4.1 Introduction

The ADC prism separation is controlled by a Galil DMC-2200 motion controller, which is in turn controlled by the ADC "dispatcher" software.The dispatcher provides all higher-level control logic, DCS monitoring and the ADC keyword service.

4.4.2 Client-side KTL Library

The ADC client-side KTL library is complete. As part of the development effort, we have automated the creation of the client library for any UCO/Lick "dispatcher2"-style service, starting from the keyword descriptions entered in the UCO/Lick "memes" database. The current set of keywords in the client library is visible at http://spg.ucolick.org/cgi-bin/Tcl/runRpt.cgi?target=k1adc&type=MemeByCon

Figure 4.4-1 shows the overall ADC architecture. The ADC dispatcher runs on the ADC host computer, monitoring a set of DCS KTL keywords that direct the ADC's action, and controlling the prism separation through the Galil. Detailed control and monitoring of the ADC is available through the ADC KTL service. The GUI uses the KTL service to provide several "views" of the ADC that are designed to be useful to the observing assistant, observer, and the instrument engineer.

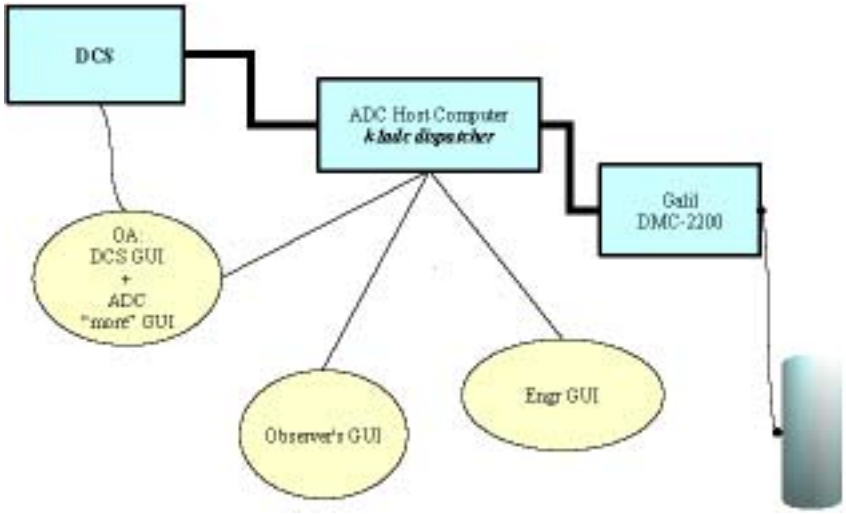

Figure 4.4-1: Overall ADC architecture. Rectangles show the main networked components, and ovals are used for user interfaces. Lines from oval boxes to rectangles indicate the main connections from GUIs to KTL services.

4.4.3 ADC Dispatcher

Communications with the DMC-2200 motion controller take place over a 100-Mbs Ethernet connection. The Ethernet connection enables the dispatcher to both read the DMC-2200's state and send new commands at a high rate, and therefore most of the control logic need not reside on board the DMC-2200 itself, but can reside in the dispatcher. This is important because the controller has limited on-board program memory, and a clumsy control language that is hard to read and harder to debug.

For the detailed design phase, we have implemented a mostly complete prototype ADC dispatcher in Tcl, rather than the C-language dispatcher originally called for in the conceptual design document. Tcl has the advantage of being a higher-level language than C, so we can develop code quickly and uncover any design problems before writing in C. Since the prototype dispatcher is running in Tcl, we have revisited the earlier decision to code the final dispatcher in C. The prototype ADC dispatcher is a solid design that can become the final ADC dispatcher with only a small amount of work. This would save one month of work compared to writing the final dispatcher in C. Tcl already serves an essential role in many existing Keck applications, such as serving KTL keywords for DEIMOS via the "infopatcher" program. The ease of development and maintenance of the package make it a good choice for the final ADC dispatcher as well as the prototype. (The use of Tcl in Keck code was addressed at the Keck SCC meeting of December 2003, in discussions that included Hilton Lewis and Al Conrad. Recognizing that Tcl is presently being used at Keck for a wide variety of critical uses, including serving KTL keywords for DEIMOS via the "infopatcher" program, it was agreed that Tcl should be treated as first-class supported language.)

The prototype dispatcher is available in the CVS repository at the location kroot/kss/Keck1ADC/k1adc/.

Compared to the ready-to-ship system, the prototype is missing these features:

a) It is controlling a Galil DMC-1800 PCI-based system rather than the DMC-2200 Ethernet-based system that will be delivered.
b) No testing has been done with DCS, since DCS has not yet been modified to support the ADC.
c) There is no real mapping function to convert between prism separation and corrected zenith angle.
d) No testing has been done with the various digital inputs that will be part of the hardware.

The design of the prototype differs in one significant way from the compared to the dispatcher design proposed in the conceptual design document: the conceptual design called for a threaded dispatcher, but the prototype is event driven. That is because the prototype is in Tcl, whereas the conceptual design anticipated a C application, and Tcl's built-in event loop makes it natural to do event-driven programming.

The prototype does retain a separate thread (actually, a co-process) for monitoring the DCS-demanded ADC mode and position. That is done because of the known problems with "DCS dropouts", in which a KTL client silently loses some of its keyword connections to DCS. We use a co-process to isolate all direct DCS interactions, making it simple to ensure that we can close and restart DCS communications without affecting the rest of the dispatcher.

The prototype itself was efficient to build, because it uses three supplementary packages to do the hard work:

1. The KTcl package is used to communicate with DCS;
2. The Traffic.tcl package is used for MUSIC messages, which is used for the k1adc service;
3. The Galil package is used for Galil communications.

The last of these is a new package, and will be posted along with the prototype dispatcher later this week. All are in the CVS repository.

The conceptual design document noted that a standalone ethernet-based Galil, such as the DMC-2200, must be able to operate safely when network communications fail. This is handled via a Galil thread that provides a deadman switch. It periodically decrements a counter; if that counter ever reaches zero, the Galil halts the motion of the motor. The dispatcher is responsible for resetting the counter at a rate at least 1 Hz. This does not affect manual (pushbutton) mode, because in manual mode the Galil is electrically disconnected from motor control. The conceptual design document also called for a temperature-monitoring thread to ensure that the electronics enclosure does not overheat, even if the dispatcher is not operating. This thread has been descoped in the detailed design, because it assumes that the ADC electronics will be placed in the HIRES enclosure, and thus the HIRES dispatchers will handle temperature control.

4.4.4 User Interfaces

The ADC requirements document did not call for any user interface. It is not a great exaggeration to say that from a user-interface perspective, the requirements document treats the ADC as a system with a simple toggle switch (tracking enabled or prisms at the null position), and therefore there was no need for any interface beyond a basic DCS control row GUI with the usual INIT/HALT/STANDBY buttons.

However, the ADC is slightly more complicated than this, and it does have more than a single on/off switch. Most of its computer-visible aspects are primarily of interest during its development and during any future trouble-shooting, and must be accessible from an engineering GUI, which would show nearly every keyword available in the system.

For example, there is a digital input to indicate if the system is in remote or local mode, if secondary limits have been reached, if various electrical cables are disconnected or broken; each of these is exposed to the engineer through keywords.

Keck has recently requested that information and control be made available through GUI's:

- If there are any problems with normal operation, the OA should have a status panel to indicate the source of the problem, and to provide detailed error messages beyond what is available in the terse DCS control row.
- The observer must be able to specify the wavelength range for which the prism separation is optimized, and to verify that the ADC is tracking the telescope elevation. The observer needn't keep this interface open, so it will not normally absorb valuable screen real estate.

It has been proposed that the GUI's be created using the "dashboard"-type interface that has been used for on all recent UCO/Lick instruments, including ESI and DEIMOS. The following figures show ideas for such an interface, provided by Greg Wirth.

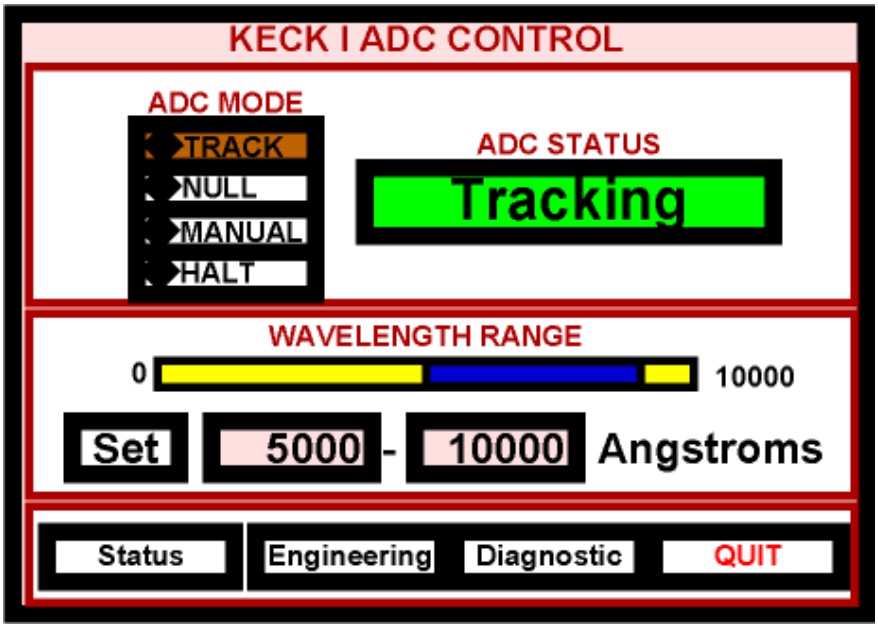

Figure 4.4-2: The main GUI panel

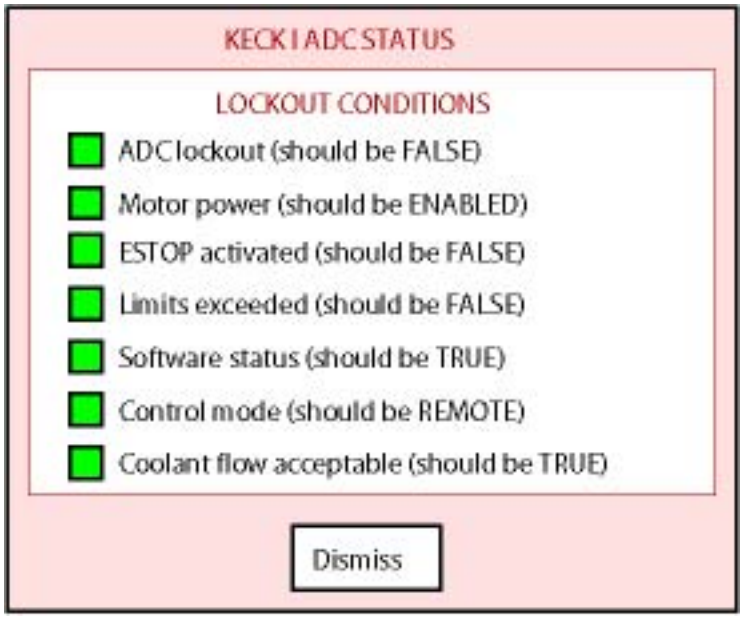

Figure 4.4-3: Sample ADC status details panel.

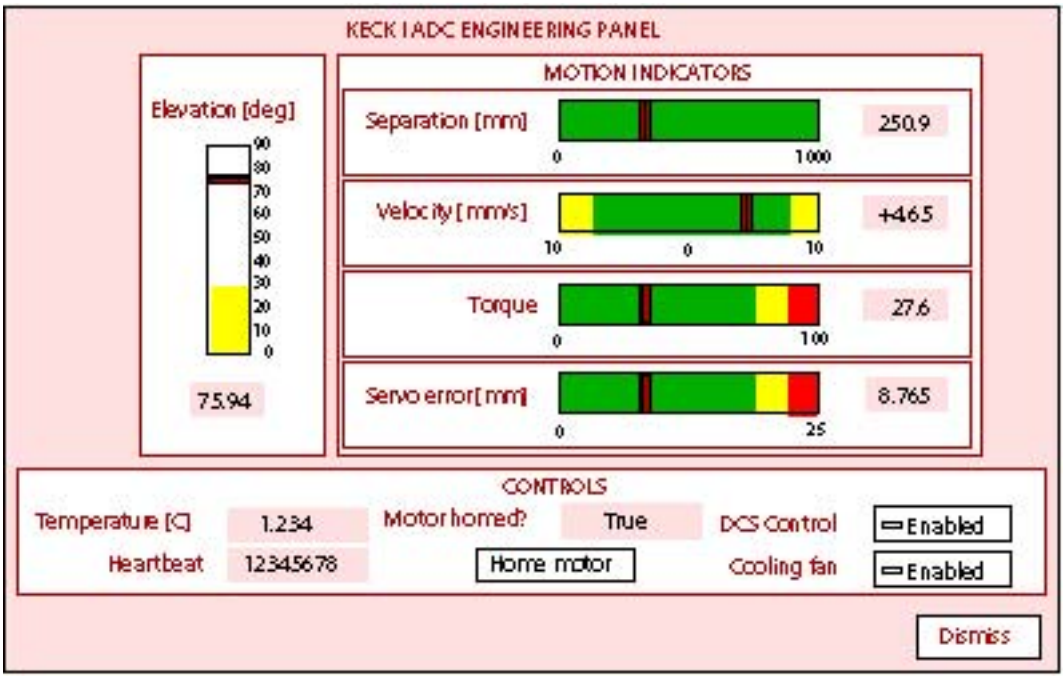

Figure 4.4-4: Sample ADC engineering panel.

It will take 1-2 weeks to implement the interface. This time will be taken from the time that was saved by not creating a C-language dispatcher, and so will not increase the overall ADC software budget.

4.4.5 Host Computer

The dispatcher runs on the ADC "host computer", which will be provided by Keck Observatory. The dispatcher's communications with the DMC-2200 take place over an ordinary network connection, and so in principle the host computer could be nearly any existing computer at the observatory.

However, the DMC-2200 is overly generous in its readiness to accept communications from any sender without verification, and we strongly urge that the motion controller be placed on an isolated private network, to avoid communications that are sent to the wrong address by mistake. To implement this, we suggest that Keck Observatory provide a host computer of its choice with two network interfaces. One of the interfaces will be connected to the observatory-wide network, and the other to the DMC-2200 private network. This computer will reside in the HIRES enclosure, and have a network connection that is not part of the HIRES instrument network.

4.5 Interface with the Keck I Telescope and Observatory Facilities

The Cassegrain ADC module has been designed to be installed into the tertiary mirror tower of the Keck I telescope using the Keck I transfer module. A full scale mock-up of the ADC module has been used to test fit the ADC through the transfer module and into the tertiary mirror tower. This has confirmed the compatibility of the ADC envelope with the ICD requirements, and has also verified the position selected for the ADC defining points that will be installed in the tertiary mirror tower.

There are small compatibility issues with the transfer module. This appears to be largely due to the way that the transfer module is aligned with the mirror tower, and small modifications to the module will be required to ensure that the ADC module can pass cleanly through the transfer module. This does not present any engineering problems.

All other envelope and handling issues related to the ADC module have been reviewed and it appears that the ADC is fully compatible with the observatory’s handling requirements.

Although it was originally proposed to locate the ADC electronics in a dedicated, cooled enclosure in the Keck I dome, finding a location for these, and also providing for connecting these electronics to the ADC module to permit servicing the ADC when it is stored on the Nasmyth deck have both proved to be a problem. As an alternative we conceived of the idea of packaging the ADC electronics in a rack insert and locating them in the electronics rack of the HIRES instrument. This rack is located in a temperature controlled locker on the right Nasmyth platform of Keck I. After verifying that this would not have an impact on the HIRES instrument, confirming available rack space, and checking the length of the cable run required to the ADC module we have concluded that this is the best solution. It also eliminates the need to supply separate glycol cooling for the ADC electronics. An analysis and/or testing will have to be done to ensure that the HIRES

electronics locker cooling can support the additional heat load, but this cooling capacity can be increased if required.

The ICD for the Cassegrain ADC has been revised to reflect these changes as well as the changes made to provide a cable connected "hand paddle" control for local operation of the ADC during telescope configuration and servicing of the ADC. The ADC electronics rack insert will be mounted on rack slides and can be removed from the HIRES electronics rack and carried to the Nasmyth deck if more extensive servicing is required.

The software control of the ADC has now been fully defined, and depending on CPU loading will either be supported by a separate small Sun workstation providing a target computer, located in the Keck I computer room, or the software will be run directly on the Keck I server. A dedicated private network connection will be used to communicate with the ADC electronics.

5 Project Schedule to Completion

Please see
http://adc.ucolick.org/fab_assy/ADC_FSD_schedule1.pdf

6 Project Budget to Completion

Please see
http://adc.ucolick.org/detailed_design/Report/ADC_FSD_budget_r2.pdf

7 Full Scale Development and Commissioning Work Plan

Please see
http://adc.ucolick.org/fab_assy/ADC_Work_Plan.pdf

8 Observatory ICD Implementation Plan

Please see
http://adc.ucolick.org/detailed_design/Report/ICD_Implementation_and_Schedule.pdf

9 Detailed Design Report Revision History

Draft: May 14, 2004
Revision 1: May 17, 2004
Revision 2: May 18, 2004
Revision 3: May 19, 2004

10 References (none)

Appendix 1

ADC Figure of Merit

Introduction:

The improved performance LRIS in spectroscopic mode with the ADC (over the no-ADC case) has many factors. Concentrating solely on spectral throughput, those factors that degrade performance without the ADC include:

1. Elevation (and its corresponding dispersion);
2. Wavelength range of interest;
3. Seeing;
4. Slitwidth; and
5. Orientation of slit with respect to the parallactic angle.

The ADC provides a correction for the dispersion, but it has some cost as well:

1. Lower transmission;
2. Slight image degradation; and
3. Residual dispersion.

Thus, the parameter space for determining a figure of merit is enormous. Here, we attempt to provide some algorithms for characterizing the effects, and provide a few representative examples.

Throughput:

The dispersion needs to be broken into two components, cross-slit (dx) and along-slit (dy) in order to estimate throughput effects. Obviously, for a given dispersion, $d(Z, \lambda)$:

$dx = d(Z,\lambda) \sin \theta$, and
$dy = d(Z,\lambda) \cos \theta$,

where θ is the angle of the slitlet with respect to the parallactic angle. The total dispersion, $d(Z,\lambda)$ is measured relative to a reference wavelength, $\lambda 0$, which also (for convenience) will be assumed to be the effective guider wavelength, and which will be assumed to fall precisely in the center of the slit. We break the relative throughput problem into a cross-slit factor, $f1(dx)$, and an along-slit factor, $f2(dy)$, both with and without the ADC.

We have used the IRAF **artdata** package to construct representative PSFs, and in turn to calculate the amount of light passing through a slit as a function of displacement of source relative to the slit center, at various slit widths and seeing. We assume a Moffat profile

PSF. Some representative throughput values are shown (Fig. 1), normalized to the maximum throughput without the ADC.

The ADC introduces some additional image size due to aberrations. We estimate the additional image size due to the ADC using the formula from the Preliminary Design Optics Report that FWHM(″) = 0.0023 R*rms*(μm); the maximum additional component due to the ADC aberrations is 0.16″. This value is added in quadrature to the original seeing size. Results for the degraded-image case are also plotted in Fig. 1, where we see that the maximum image degradation leads to a reduction of the peak value by a few percent at most, and affects only the results in the center of the slit.

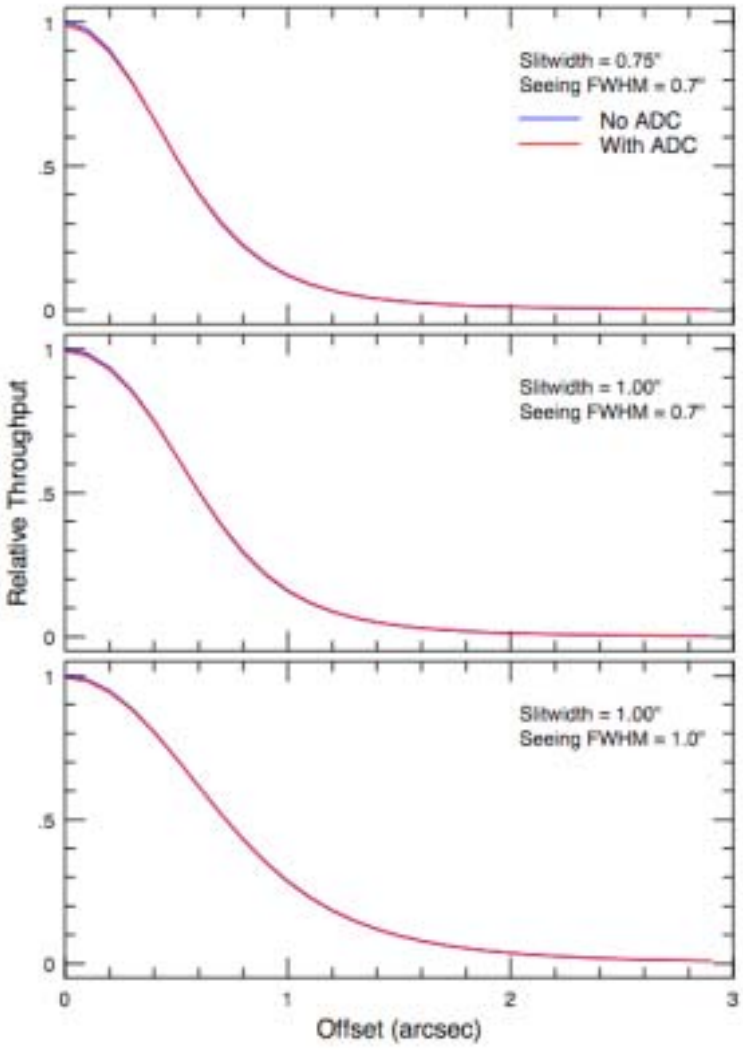

Figure 1: Throughput (relative to no-ADC case) as a function of distance from the slit center. The ADC case shown differs only in slightly lower central throughput, due to slightly larger images.

We can now estimate the throughputs with and without the ADC for the cross-slit direction by using these curves and calculating the displacement from the relative dispersion at the desired elevation, and applying the geometrical factor, sin θ. Thus,

$f1(\lambda) = E(dx)$,

where *E* represents the throughput from the figures. In the case of the ADC, the residual dispersion is used in place of the native dispersion.

Even with perfect alignment between slitlet and parallactic angle, dispersion can still reduce efficiency because a longer slitlet is needed to capture the light. This is purely a geometrical effect, and loss of efficiency can be crudely approximated by a factor

$f2 = \langle slitlen \rangle / (\langle slitlen \rangle + |\Delta dy|)$,

where Δdy represents the total range in the dispersion or residual dispersion. Effectively, slits must be longer and so fewer objects can be observed (note: this tends to be relevant only where target density on the sky is relatively high).

In addition to the two factors above, the ADC includes additional transmission; we describe this as an additional factor, $f3(\lambda)$, which is everywhere > 0.96.

In summary, the spectral throughput without the ADC relative to that with it is given by

$$R = f1(\lambda) \times f2 / (f1^{ADC}(\lambda) \times f2^{ADC} \times f3^{ADC}(\lambda)),$$

where R depends on seeing, slitwidth, Z, λ, λ0 and θ. We use these functions in the calculations below. Note that the ADC residual dispersion is never greater than 0.2 arcsec, so that $f2^{ADC} \approx 1$ and $f1^{ADC}(\lambda) \approx$ (1 – few%) due to slightly larger image size with the ADC.

Examples:
We consider some representative cases:

1. Zenith distances of 20, 40 and 60 degrees;
2. Seeing FHWM 0.7 and 1.0 arcseconds;
3. Slitwidths 0.75 and 1.0 arcseconds;
4. Mismatches of 20 and 70 degrees between slit and parallactic angle. A 20 degree mismatch is probably as good as an observer can expect under normal circumstances, as masks are never used at precisely the design time, particularly given typically long exposure times (1—1.5 hours total); and
5. A slit-length of 15″, chosen as a relatively conservative length in calculating f2.

The results are shown graphically in Fig. 2. The drop in relative throughput at the reference wavelength (λ0 = 0.42 μm) is due to *f*2, i.e., the need for increased slit lengths. It is interesting to note that even at high elevation (Z=20°), there is effectively no disadvantage

to using the ADC, and at even modest zenith distances (Z=40°), the ADC correction in the *well-oriented case* provides improvements of 10—20% in throughput. In all cases, the larger images for the fully-extended ADC are used; in practice, the ADC performance at Z=20° and 40° is better than shown by 1—3%.

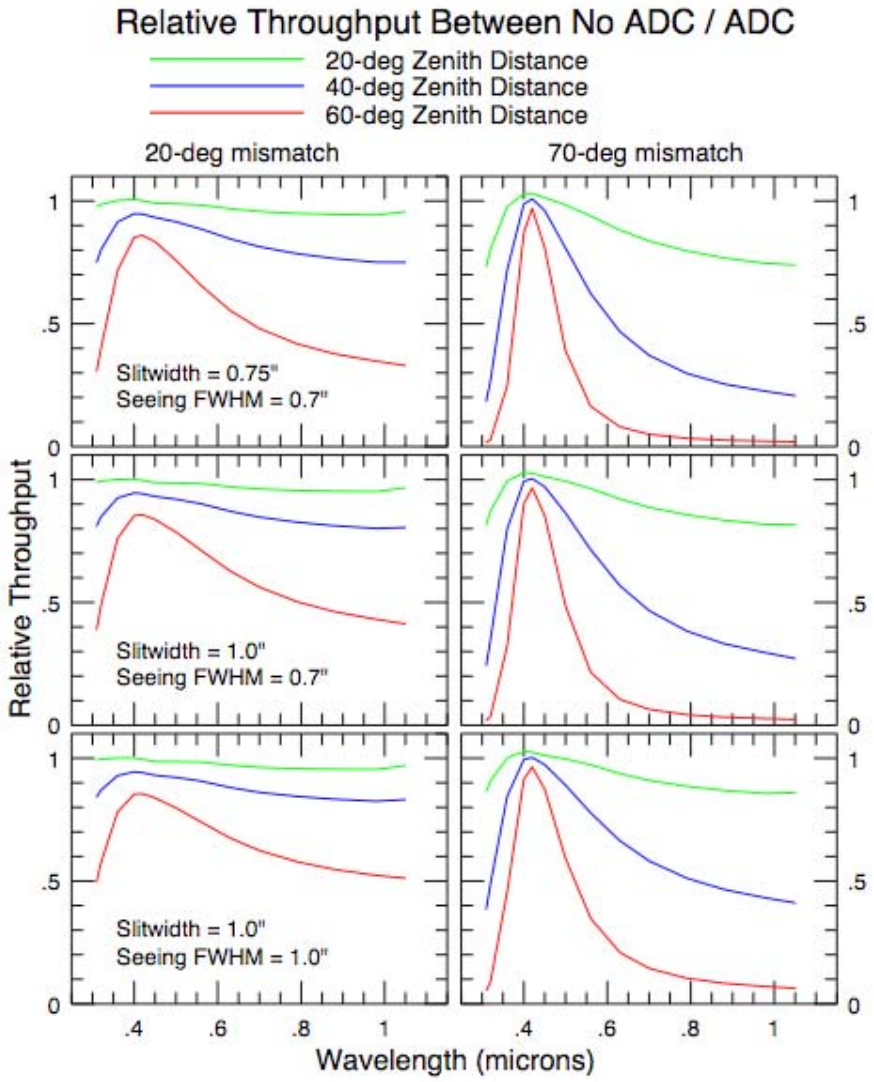

Figure 2: Relative Throughputs, comparing the non-ADC case against the ADC case. Left column shows slits well-oriented with the parallactic angle, right column poorly-aligned. Three elevations are shown in each plot. The decline in throughput at 0.42-μm is due to the need for longer slitlets in the non-ADC case; a slit length of 15″ is assumed.

Other Considerations Not Related to Throughput:

These effects may have serious consequence to the science without effecting throughput:

1. An exposure of significant duration may cover a range of dispersions as elevation changes. At the effective wavelength of the guider, this will have no effect on the spectrum. At other wavelengths, a blurring due to the changing dispersion will occur. For example, assume perfect alignment between slit and the parallactic angle, and that the guider has an effective wavelength of 7000A. Suppose the relative dispersion between 3500A and 7000A changes by 0.3 arcsecond during the exposure. This means that the spectrum at 3500A will drift 0.3 arcsecond in the spatial direction over the course of the exposure, lowering the contrast and changing the spatial profile. Such a situation can occur in less than a 4-degree change in elevation near Z=60-deg.
2. The distribution of the source light within the slit can have serious ramifications for precision radial velocity work. Dispersion can cause the light distribution within the slit to change at different wavelengths, producing systematically different velocity measurements at different wavelengths. Similarly, for extended objects such as galaxies, different portions of the object will be sampled at different wavelengths if there is any dispersion in the cross-slit direction.